WAVELET BASED DENOISING OF ECG AND ICG SIGNALS

A dissertation submitted in

partial fulfillment of the requirements for the degree of

Master of Technology

by

Toney Sebastian

(09330009)

under the supervision of

Prof. P. C. Pandey

Biomedical Engineering Group

Department of Biosciences and Bioengineering

Indian Institute of Technology Bombay

June 2011

Indian Institute of Technology Bombay

M. Tech. Dissertation Approval

This dissertation entitled **"Wavelet Based Denoising of ECG and ICG Signals"** by **Toney Sebastian** (Roll No. **09330009**) is approved, after the successful completion of *viva voce* examination, for the award of the degree of **Master of Technology in Biomedical Engineering**.

Supervisor	....	(Prof. P. C. Pandey)
Examiners	....	(Prof. S. Mukherji)
	....	(Prof. V. Rajbabu)
Chairperson	....	(Prof. K. M. Moudgalya)

Date: 28 June, 2011

Place: Mumbai

Declaration

I declare that this written submission represents my ideas and my own words and where other's ideas or words have been included, I have adequately cited and referenced the original sources. I also declare that I have adhered to all principles of academic honesty and integrity and have not misrepresented or fabricated or falsified any idea/data/fact/source in my submission. I understand that any violation of the above will be cause for disciplinary action by the Institute and can also evoke penal action from sources which have thus not been properly cited or from whom proper permission has not been taken when needed.

Toney Sebastian

Toney Sebastian

Date: 28 June, 2011

Place: Mumbai

Toney Sebastian / Prof. P. C. Pandey (Supervisor), "Wavelet Based Denoising of ECG and ICG Signals", *M. Tech. dissertation*, Biomedical Engineering Group, Department of Biosciences and Bioengineering, Indian Institute of Technology Bombay, June 2011.

ABSTRACT

The electrocardiogram (ECG) and impedance cardiogram (ICG) are biosignals related to the functioning of the heart. Impedance cardiography is based on sensing the variation in the thoracic impedance caused by variation in the blood volume in the thorax. The respiratory and motion artifacts in the sensed signal introduce errors in the estimation of the stroke volume and other cardiovascular indices. A wavelet-based denoising technique, using discrete Meyer and symlet-26 wavelets, for suppressing these artifacts was investigated. It uses scale-dependent thresholding for suppressing the respiratory artifact and limiting of the wavelet coefficients for suppressing the motion artifact. Denoising of ICG signals with simulated respiratory artifacts of -9 dB resulted in an SAR improvement of 23.5 dB, and L_2 norm and max-min based improvement indices close to one. Denoising of ICG recordings with respiratory and motion artifacts resulted in improvement indices of value close to one, indicating that artifacts were suppressed without introducing any significant distortion in the signal. Wavelet-based denoising was also investigated for suppressing the EMG noise and the motion artifact in ambulatory ECG. EMG noise is reduced by thresholding the wavelet coefficients using an improved thresholding function combining the features of hard and soft thresholding. Motion artifact is reduced by limiting the wavelet coefficients. Thresholds for both the denoising steps are estimated using the statistics of the noisy signal. Denoising of simulated noisy ECG signals with -10 dB input SNR resulted in an average SNR improvement of 11.4 dB, and its application on ambulatory ECG recordings resulted in L_2 norm and max-min based improvement indices close to one, indicating that the technique was effective in denoising without introducing any significant signal distortion. Its application significantly improved automated R-peak detection.

CONTENTS

List of Figures

List of Tables

List of Abbreviations

AFER	Adaptive filtering by using estimated respiration
AFSR	Adaptive filtering by sensing respiration
CWT	Continuous wavelet transform
DWT	Discrete wavelet transform
ECG	Electrocardiogram
EMG	Electromyogram
FIR	Finite impulse response
ICA	Independent component analysis
ICG	Impedance cardiogram
II	Improvement index
IIR	Infinite impulse response
IMFs	Intrinsic mode functions
LMS	Least mean square
PCG	Phonocardiogram
RMS	Root mean square
SAR	Signal-to-artifact ratio
SNR	Signal-to-noise ratio
TI	Translation-invariant

List of Symbols

a_i	Approximation at the i^{th} scale
d_i	Detail at the i^{th} scale
$D(n)$	Unmodified wavelet coefficients
$\hat{D}(n)$	Modified wavelet coefficients
p90	90^{th} percentile
$r_o(n)$	ICG-free respiratory artifact
S_i	Transition span
$s(n)$	Artifact-free ICG
T_{lvet}	Left ventricular ejection time
$x(n)$	Unprocessed ICG
$\hat{x}(n)$	Processed ICG
$\hat{x}_m(n)$	m^{th} level partial reconstruction
$Z(t)$	Total sensed thoracic impedance
α	Scaling factor
$\gamma(n)$	Scaling factor for threshold estimation
η	Denoising control factor
$\theta(n)$	Time-varying threshold for modified thresholding
μ	Mean
σ	Standard deviation
ϕ_i	Threshold for limiting

Chapter 1
INTRODUCTION

1.1 Problem Overview

The electrocardiogram (ECG) and impedance cardiogram (ICG) are biosignals related to the functioning of the heart [1]–[6]. These cardiac biosignals are generally corrupted by artifacts, which may be much stronger than the signal during ambulatory and post-exercise recordings. As the presence of the artifacts may make it difficult to get the desired diagnostic information, it is important to suppress them. ECG is a measure of electrical activities of the heart which is obtained by placing surface electrodes at specific locations of the body [4]–[6]. An ambulatory ECG records the electrical activates of the heart while performing normal activities. Such a recording has great importance in clinical practice as many of the cardiac disorders may not be observable in ECG recorded under a resting state. These recordings get affected by several disturbances. The major disturbances are baseline wander, powerline interference, electromyogram (EMG) noise, and motion artifact [5], [6]. Powerline interference and baseline wander can be reduced by a careful design of the ECG hardware. EMG noise is the interference produced by the skeletal muscles during their contraction. These signals severely affect the ECG because of the overlap in their spectra. The ECG signals have components in the range of 0.01 Hz to 250 Hz and the myopotential spectrum extends from 20 Hz to 10 kHz [5], [6]. Motion artifact is the disturbance, due to changes in the half-cell potential of the electrodes, caused by motion related electrode movement and stretching of the skin under the electrode [6]–[8]. It appears as irregular baseline wander in the ECG and looks similar to the P wave or the R wave. The artifacts in ECG make it difficult to detect the characteristic features like P wave, elevation or dip of the ST segment, etc. The performance of most of the automated feature extraction and signal compression algorithms may get affected by the artifacts [8]–[13]. Motion artifact and EMG noise can be minimized by restricting the motion of the patient during signal recording, but this is not possible in ambulatory ECG recording. Signal processing techniques for ECG denoising, are generally employed for suppressing these disturbances [6]–[14].

Impedance cardiography is a noninvasive technique based on sensing the variation in the thoracic impedance $Z(t)$ caused by variation in the blood volume in the thorax [1]–[3]. The thoracic impedance and the variations in it are sensed by injecting a high-frequency low amplitude current into the thorax region through a pair of electrodes and picking-up the resulting amplitude modulated voltage across the same or another pair of electrodes. The negative of the time derivative of $Z(t)$ is known as the ICG [1], [2]. The parameters obtained from ICG can be used to estimate the stroke volume and some other cardiovascular indices and for obtaining diagnostic information. Figure 1.1 shows an example of $Z(t)$ and the ICG waveforms ($-dZ/dt$) along with the associated ECG and phonocardiogram waveforms. The ICG waveform has four main characteristic points: B, C, X, and O. The B point and the X point indicate the opening and closing of the aortic valve, respectively. The time duration between the B point and the X point gives the left ventricular ejection time (T_{lvet}). The C point corresponds to the point of maximum rate of impedance change $(-dZ/dt)_{max}$, which approximately indicates the peak blood flow in the ascending aorta [1]. The O point indicates the opening of the mitral valve. The left ventricular ejection time and the peak value of the ICG are used to calculate the stroke volume, using the Kubicek's formula [1], [2] or one of its modifications [3].

The ICG signal is generally influenced by respiratory and motion artifacts, which may be much stronger than the signal during exercise and post-exercise recordings [2], [16]–[22]. The thoracic impedance signal generally has a cardiac component of 0.15–0.2 Ω, while the respiration related changes are in 0.5–2 Ω range [23]. The bandwidth of the ICG signal extends over 0.8–20 Hz while respiratory and motion artifacts have components in the range 0.04–2 Hz and 0.1–10 Hz, respectively [20], [22]. As the artifacts in ICG introduce errors in the estimation of the stroke volume and other cardiovascular indices, it is important to suppress them. Motion artifact can be avoided by acquiring the signal with the patient lying in a resting state. Holding of the breath during the recording can be used to avoid respiratory artifact, but it may affect the stroke volume and it can not be used for recording over a long

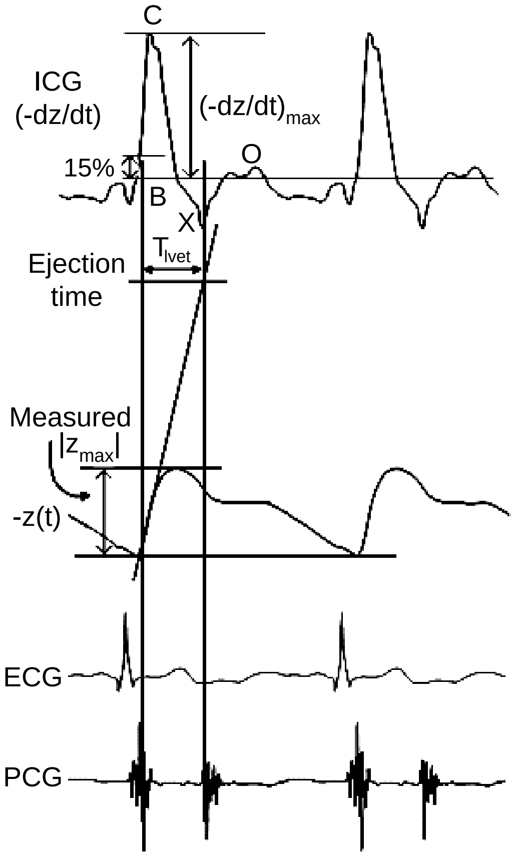

Fig. 1.1 Impedance cardiography waveforms -*dZ*/*dt* and -*z*(*t*) along with the associated ECG and phonocardiogram (PCG), and forward-slope extrapolation for calculating ΔZ [15].

interval from most patients. Therefore it is important to investigate suitable denoising technique for the suppression of these artifacts.

1.2 Project Objective

The aim of this project is to investigate denoising techniques for suppression of respiratory and motion artifacts from ICG signals and suppression of EMG noise and motion artifact from the ambulatory ECG signals. The denoising method should not need any reference input, and automated detection of characteristic features should be possible after denoising. Earlier work in our lab [15], [21], [24] showed that the wavelet-based denoising techniques have potential to meet these objectives and hence it was decided to carry out detailed investigation on their use in denoising the ECG and ICG signals.

Respiratory artifact in ICG is suppressed using scale-dependent thresholding. Effectiveness of different wavelets for the suppression of respiratory artifact is studied. EMG noise in ambulatory ECG is suppressed by thresholding wavelet coefficients with thresholds estimated using modified thresholding functions, by combining the features of soft and hard thresholding. Translation invariant filtering is used for the suppression of oscillations due to Gibbs phenomenon. A technique based on limiting the wavelet coefficients is developed for the suppression of motion artifact in ICG and ambulatory ECG. Effectiveness of modified limiting functions in motion artifact suppression is also investigated.

The effectiveness of the denoising techniques is assessed by applying them on signals with simulated artifacts and also on signals acquired from several healthy volunteers during different physical activities.

1.3 Report Outline

Chapter 2 presents a review of the techniques for denoising of ICG and ECG signals. The investigations on the ICG denoising are presented in Chapter 3 and the investigations on the ECG denoising are presented in Chapter 4. A summary of the work, conclusions, and some suggestions for future work are given in the last chapter.

Chapter 2
DENOISING TECHNIQUES

2.1 Introduction

This chapter gives a review of some of the ICG and ECG denoising techniques. Artifact suppression in ICG using ensemble averaging, adaptive filtering, linear filtering, and wavelet based techniques are reviewed in Section 2.2. Various ECG denoising techniques like adaptive filtering, non-linear filtering, and denoising techniques based on wavelets and empirical mode decomposition are reviewed in Section 2.3.

2.2 ICG Denoising

The ICG signal is generally influenced by respiratory and motion artifacts, which makes automated detection of the characteristic points difficult, and hence introduces errors in the calculation of various cardiovascular indices. Several signal processing techniques have been reported for the suppression of respiratory and motion artifacts in ICG [15]–[23], [25]–[27]. Ensemble averaging of the ICG with respect to the R-peaks of ECG is the most commonly used method for reducing the artifacts [16], [19], [25], [26]. But it also suppresses the beat-to-beat variations in ICG and may introduce errors in the estimation due to smearing of the characteristic points in the waveform [8].

Riese *et al.*, [26] used a large-scale ensemble averaging technique for the ambulatory impedance cardiogram. They used an accelerometer based device, sensitive to the changes in vertical acceleration to sense the gross body movements. Each subject was asked to keep an activity diary, using the entries in the activity diary and the signal from the accelerometer, the entire record was divided into fixed periods (i.e., periods with fixed activity, posture, physical load, location, and social situation) of maximally one hour. They applied the large scale ensemble averaging on the ICG with respect to the ECG R-wave. The method introduced distortions by attenuating the amplitudes of peaks and troughs of the ICG waveform. The technique also resulted in suppressing the beat-to-beat variability in the cardiac parameters.

Yamamoto *et al.* [22] designed and implemented a digital IIR band-pass filter, centered at the heart rate, for real-time suppression of the respiratory artifact. The associated ECG and changes in thoracic circumference were also simultaneously measured along with the ICG. The IIR filter was designed in such a way that the gain of the filter at the center frequency was set to 0 dB. At the respiration frequency the gain was set to -20 dB. The filter had a sharp band-pass characteristics with the center frequency could change adaptively to follow the heart rate variability. However, it introduces nonlinear phase distortion and may attenuate high frequency components of the ICG signal.

Raza *et al.* [23] used a digital IIR high-pass filter with voluntary cardio-respiratory synchronization (heart rate and respiration in the ratio of 5:1), with the cutoff frequency automatically varying as a function of the heart rate. To avoid the nonlinear phase shift, they used forward filtering followed by backward filtering. However, voluntary cardio-respiratory synchronization is not possible during exercise and post-exercise measurements and is difficult for patients with high heart rate variability. The technique may also introduce distortion in the ICG signal during exercise and post-exercise recordings because of the high frequency components in the artifact.

Barros *et al.* [17] developed an adaptive filter with scaled Fourier linear combiner, with a reference signal related to the R-R interval of the ECG for the suppression of non-correlated noise in impedance cardiography. They modeled the ICG signal as a Fourier series with a period equal to the R-R interval, and the coefficients were estimated using the LMS algorithm. It may result in distortion due to the variation in time difference between the electrical and mechanical activities of the heart.

Pandey and Pandey [15], [27] proposed an LMS-based adaptive filtering technique (AFSR), with the simultaneously acquired respiratory signal as the reference for the suppression of respiratory artifact. The respiratory signal was acquired using a thermistor based airflow sensor placed in front of the nostrils. An SAR improvement of 18.5 dB was reported for signals with simulated artifact with the input SAR in the range of -9 to 9 dB. The output of the respiration sensor was deficient in higher frequencies, and hence the technique was not effective in suppressing higher spectral components of the respiratory artifact, which may severely affect the detection of characteristic points in the ICG waveform. To overcome this drawback they proposed another LMS based adaptive filtering technique (AFER) with the estimated respiration as the reference signal [15]. The reference signal was estimated using the sensed respiration and the sensed impedance, using a cubic spline fitting on the ICG waveform. An SAR improvement of 19.6 dB was reported, and the technique was also effective in suppressing the higher frequency components of the artifact. The technique facilitates calculation of the stroke volume without suppressing the beat-to-beat variability during post-exercise measurements.

Several wavelet based techniques have been reported for denoising of biosignals [15], [21], [24], [28]–[31]. Ouyang *et al.* [31] reported denoising techniques based on continuous wavelet transforms (CWT) and discrete wavelet transform (DWT) for the suppression of respiratory artifact in ICG. Marr wavelet was used to decompose the signal into different levels using continuous wavelet transform and some of the higher scales were abandoned to suppress the respiratory components and the artifact suppressed signal was reconstructed using the remaining scales. Because large number of scales are required, CWT based denoising is computation intensive. Another problem with this technique is number of scales used for reconstruction are not fixed. The DWT based technique used soft thresholding for the suppression of respiratory artifact. The sensed signal had both respiratory and cardiac components. It was passed through a pre-whitening filter to suppress the cardiac component. The filter was obtained by taking the inverse of an auto-regressive model of the cardiac component. The processed signal was then decomposed into seven levels using Coiflets wavelet (order 5), followed by soft thresholding to get the modified coefficients. The soft thresholding suppresses the whitened cardiac components. The modified coefficients were subtracted from the original coefficients, which were then processed using the inverse of the pre-whitening filter. The DWT based method resulted in an SNR improvement of 30.3 dB for simulated signals at an input SNR of -15 dB. In [15], [21], scale-dependant thresholding using discrete Meyer wavelet has been used for suppression of the respiratory artifact in the ICG sampled at 500 Hz. The ICG signal was decomposed into ten levels using FIR based Meyer wavelet (dmey) and the artifact suppressed signal was reconstructed by adding the first eight details. An SAR improvement of 21.8 dB was reported for signals with simulated artifact with the input SAR in the range of -9 to 9 dB. The filter length of dmey wavelet is 102, it may be possible to get the same results as obtained by [15], [21] by using some other wavelets with lesser number of filter coefficients and thereby reducing the computations.

In wavelet-based denoising applications, selection of the wavelet basis, thresholding technique, and the estimation of the thresholds are important. The noise suppression is better if the shape of the wavelet or its scaling function closely matches the shape of the signal or the noise. If the signal components of the input noisy waveform are restricted to a few details, these can be added together to reconstruct the denoised signal. Hence various wavelets need to be evaluated for their suitability for suppressing the respiratory artifact. The wavelet thresholding is based on the assumption that noise components are always present and that the noise amplitudes are low in comparison with the signal, and hence the contribution of the signal and noise to the wavelet coefficients can be separated on the basis of the magnitude of the coefficients as a function of time [32]. These assumptions are not valid in the case of motion artifact in ICG, because the signal components are always present and the motion artifact may be intermittent and may be stronger than the signal.

A wavelet-based technique for suppressing the respiratory and motion artifacts in impedance cardiography has been developed. It uses scale-dependent thresholding for suppression of respiratory artifact and wavelet coefficient limiting for suppression of motion artifact. Use of various wavelet functions and methods for estimating the thresholds are empirically investigated. Detailed description of the denoising technique is given in Chapter 3. The effectiveness of the denoising is assessed by applying it on ICG signals with simulated artifacts and on ICG signals acquired from several healthy subjects during different physical activities and exercises.

2.3 ECG Denoising

Motion artifact and EMG noise have a spectral overlap with ECG and they cannot be effectively suppressed by filtering [5]–[10]. Tong *et al.*, [7] used an LMS based adaptive filter for reducing motion artifact with the output of an accelerometer, placed on the ECG electrode on the right arm, as the reference input. They used two motion sensors, a two-axis anisotropic magnetoresistive sensor and a three-axis accelerometer. A low pass filter was included in the system to reduce the magnitude of the QRS complexes in the noisy ECG signal prior to the adaptation. Use of accelerometer resulted in better performance than that of the magnetoresistive sensor. The filter was not effective in suppressing the low-level noise, which may introduce errors in automated ECG analysis.

He *et al.* [8] used a method based on independent component analysis (ICA) on 3-lead ECG. ICA can be used to separate a signal into *m* independent components using *m* simultaneous observations of the signal based on the assumption that the signal and noise are statistically independent. The authors applied ICA on 3-lead ECG and estimated three independent components. The components representing noise were automatically identified using kurtosis with an empirically selected threshold, and set to zero and the remaining components were mixed back to get the denoised set of observations. The technique may not be effective if all the three channels are corrupted with noise and cannot be applied to single-lead ECG. Dai and Lian [10] used modified moving window averaging to estimate and remove baseline wander from ECG, by applying the moving average on samples separated by intervals rather than on consecutive samples and by removing the samples corresponding to the R-peaks.

Blanco -Velasco *et al.* [13] used empirical mode decomposition for denoising ECG. The input ECG was decomposed into its fundamental oscillations, called intrinsic mode functions (IMFs). The initial IMFs were related to high frequency noise and QRS complexes. The noise in the initial IMFs was separated by windowing out the R-peak locations. A low-pass filter bank was used to extract the baseline wander from final IMFs. The extracted disturbances were subtracted from the input ECG to get the denoised signal. Since time domain windowing is used to preserve the QRS complex, the technique cannot suppress the artifacts in this region.

Several techniques using wavelet-based multi-resolution analysis have been reported for denoising ECG signals [28], [29], [33]–[35]. Zhang [28] applied wavelet decomposition using symlet (order 10), which has a shape similarity to the QRS complex, for removing the baseline wander from the ECG signal sampled at 360 Hz, by subtracting its eighth scale approximation. It resulted, at times, in a distortion in the ST segments. The EMG noise was removed by wavelet thresholding. Out of the several methods studied, the best results were obtained by using EBayes threshold. Denoising was found to be better for piecewise thresholding than for processing the whole record together. Li and Lin [35] reported that EMG noise could be consistently suppressed by hard thresholding with EBayes threshold with 5-level decomposition using symlet (order 4). Features of both the hard thresholding and soft thresholding can be combined by suitably designing the thresholding function [29], [36]. It has been reported that thresholding the wavelet coefficients may result in oscillations at sharp transitions in the signal due to Gibbs phenomenon, and that it can be reduced by using translation-invariant denoising [28], [29].

The wavelet-based denoising techniques generally employ hard, soft, or improved thresholding functions with the thresholds obtained using SURE, EBayes, Donoho's universal threshold, *etc.* These techniques produce good signal enhancement for noises which are uniformly present throughout the signal, but they are not effective in suppressing real EMG noise. The motion artifact is generally suppressed by eliminating approximation at a particular scale, but it may cause signal distortion or improper artifact correction. To overcome these problems, a technique using an improved thresholding function and limiting of the wavelet coefficients for suppressing EMG noise and motion artifact, respectively, is investigated. Thresholds for both the denoising steps are estimated using the statistics of the noisy signal itself. The technique is validated by applying it on noisy ECG signals generated using the records from the MIT/BIH database [37]–[39] and on ambulatory ECG recordings. The details of the technique and results are presented in Chapter 4.

Chapter 3
WAVELET BASED DENOISING OF ICG

3.1 Introduction

This chapter presents a wavelet based technique for the denoising of ICG signals. The advantage of wavelet-based method is that it does not require a reference signal. A technique involving scale-dependent thresholding for the suppression of respiratory artifact and limiting of wavelet coefficients for the suppression of motion artifact is investigated [42]. All the analysis and processing were carried out using Matlab. The denoising technique is described in Section 3.2 followed by the method of evaluation and results.

3.2 Denoising of ICG

Pandey [15] reported that scale-dependent thresholding using discrete Meyer (demey) wavelet can be employed for suppression of respiratory artifact in ICG sampled at 500 Hz. It may be possible to get similar performance by using some other wavelets with lesser number of filter coefficients and thereby reducing the calculation complexity. With this perspective, we have investigated the effectiveness of different wavelet bases from Daubechies, Coiflets, discrete Meyer (dmey), and symlet families in separating respiratory artifacts and ICG. These wavelets and the associated scaling functions are shown in Fig. A.1 in Appendix A. Ten-level decomposition of the artifact-free ICG signals and the ICG-free respiratory artifacts, showed that dmey and symlet-26 (sym26) captured the ICG in its first few levels and the artifact component in the other levels. They were effective in compactly representing the signal and the artifact. For ICG sampled at 500 Hz, the signal components were present in details up to D8, and these details did not show contribution from respiratory artifact. Thus scale-dependent thresholding using dmey and sym26 is used for the suppression of respiratory artifact in the ICG. The denoised signal is reconstructed by adding together the first eight details.

Ten-level decomposition of the noise-free ICG signals, using dmey, showed all the coefficient magnitudes to be below a certain value. In the presence of motion artifact, some of the coefficients acquired much higher values. Hence it may be possible to suppress motion artifact by limiting the coefficient magnitude at a threshold value called the limiting threshold. Several statistical methods, like SURE, universal threshold, Empirical Bayesian, minimax, etc. have been used earlier for thresholding-based denoising [28]–[30], [32]. Minimax threshold is the largest threshold that minimizes the maximum relative risk [32]. Its use produced limiting threshold values which effectively suppressed motion artifact represented in D5–D8. The values of the estimate of threshold by this method is directly proportional to the number of samples processed and hence results in higher threshold values for lower scales (D1–D5) as they have higher number of coefficients. Coefficient limiting of these scales using minimax thresholds doesn't result in significant artifact suppression as the values of the estimated thresholds are higher. Hence use of "level dependent" thresholding is investigated for the suppression of motion artifacts from these scales.

In artifact-free recordings, the wavelet coefficients in lower scales (D1–D5) were found to be almost uniformly distributed. For signals with strong motion artifact, the coefficients representing motion artifact had relatively higher values and were easily distinguishable from those representing the signal components. For these scales, "level-dependent" thresholds can be estimated for limiting. For this purpose, the coefficients are divided in frames of two times the average R-R interval, ensuring at least one complete cardiac cycle in every frame. The R peaks are located by applying the Pan-Tompkins algorithm [11] on simultaneously acquired ECG. In each frame, the absolute maximum is found for each scale. The maxima in all the frames are used to calculate mean μ_i and standard deviation σ_i for each scale *i*. The threshold for wavelet limiting is taken as $\mu_i - \eta\sigma_i$. A value of η close to 0 resulted in effective denoising without causing signal distortion, while a larger value caused distortion in artifact-free ICG segments. Based on the above empirical investigations for suppressing motion artifact, minimax-based thresholds were used for D5–D8, while level-dependent thresholds were used for D1–D5, with D5 subjected to two limiting operations. It has been earlier reported that thresholding-based denoising of

ECG results in oscillations at sharp transitions in the signal and these can be suppressed by translation-invariant application of the denoising [29]. Such oscillations were not visible in the denoised output after application of either of the two denoising steps of our technique.

3.3 Method of Evaluation

The ICG signals for the study were recorded using the impedance cardiograph developed in our lab [15], [40] and the impedance cardiograph model HIC2000 (from Bio-impedance Technology, Chapel Hill, NC) at a sampling rate of 500 Hz. Two sets of signals were used for the evaluation. In set A, three types of signals were recorded from two healthy subjects: (i) subject holding the breath, in resting state (artifact-free recording), (ii) subject in resting state without any restriction on breathing (recording with respiratory artifact but no motion artifact), (iii) subject performing different physical activities (recording with both types of artifacts). Set B consisted of signals with simulated artifacts [15], [40]. For this purpose, two types of signals were recorded from healthy volunteers, with the volunteer resting in supine position without any non-ventilatory movements. During the first recording, the volunteer held the breath for 10 s. One of the cycles was repeatedly concatenated to obtain a periodic artifact-free ICG. During the second recording, the volunteer synchronized the inhale and exhale phases with 0.4 Hz square wave displayed on an oscilloscope. Sixty cycles of the ICG were ensemble averaged with respect to the respiratory cycle to estimate one cycle of respiratory artifact. It was repeatedly concatenated to simulate a periodic ICG-free respiratory artifact. The ICG-free artifact was scaled to have the same RMS value as the artifact-free ICG signal. The ICG-free artifact $r_0(n)$ was added to the artifact-free ICG $s(n)$ with a scaling factor α to obtain the contaminated ICG

$$x(n) = s(n) + \alpha\, r_0(n) \tag{3.1}$$

with a signal-to-artifact ratio (SAR) of $-20\log\alpha$. These signals were recorded by Pandey [15], as part of his research in our lab. Twenty such records were used.

A quantitative evaluation for selecting the most suitable wavelet for respiratory artifact suppression was carried out by using the artifact-free set of signals in set A and by estimating the RMS error in reconstructing the signal. The denoising was qualitatively evaluated by a visual examination of the output for suppression of the artifacts and presence of distortion in the signals in set A. For quantifying the respiratory artifact suppression, the technique was applied on set B of signals. The SAR in the N-sample segment of output $\hat{x}(n)$ after denoising was calculated as

$$SAR_{out} = 10 \log \left(\sum_{n=1}^{N} s^2(n) \;/\; \sum_{n=1}^{N} \left|\hat{x}(n) - s(n)\right|^2 \right) \tag{3.2}$$

The evaluation based on improvement in SAR can be used only for signals with simulated artifact. Another evaluation, as used by Tong *et al.* [7], involved the improvement indices (II) based on L_2 norm and excursion (max-min) of the signal and calculated as

$$\text{II} = \frac{\left|(\text{Pre-denoising value}) - (\text{Post-denoising value})\right|}{\left|(\text{Pre-denoising value}) - (\text{Artifact-free value})\right|} \tag{3.3}$$

It can be computed for signals with actual artifacts by using an artifact-free segment as the reference. An index value close to one indicates an effective denoising and a small value indicates ineffective noise suppression. A value larger than one indicates signal distortion.

3.4 Results

Ten-level decomposition of artifact-free ICG (from the set A of signals) and ICG-free respiratory artifact (from the set B of signals) using dmey and sym26 wavelets showed that ICG was captured in the first eight details and respiratory artifact in the last two details and the approximation A10. An example of the ten-level decomposition of an artifact-free ICG signal using dmey and sym 26 wavelets is given in Fig. 3.1. It can be seen that the last two details and the approximation A10 do not have any significant signal components. Figure 3.2 shows the ten-level decomposition of an ICG-free respiratory artifact using dmey and sym26 wavelets. It can be observed that the artifact components are dominated in the last two details and the approximation. For a quantitative evaluation an artifact-free ICG from set A and an ICG-free artifact from set B were decomposed into ten levels such that

$$x(n) = \sum_{i=1}^{10} d_i(n) + a_{10}(n) \tag{3.4}$$

where d_i and a_i are detail and approximation, respectively, at the i^{th} scale.

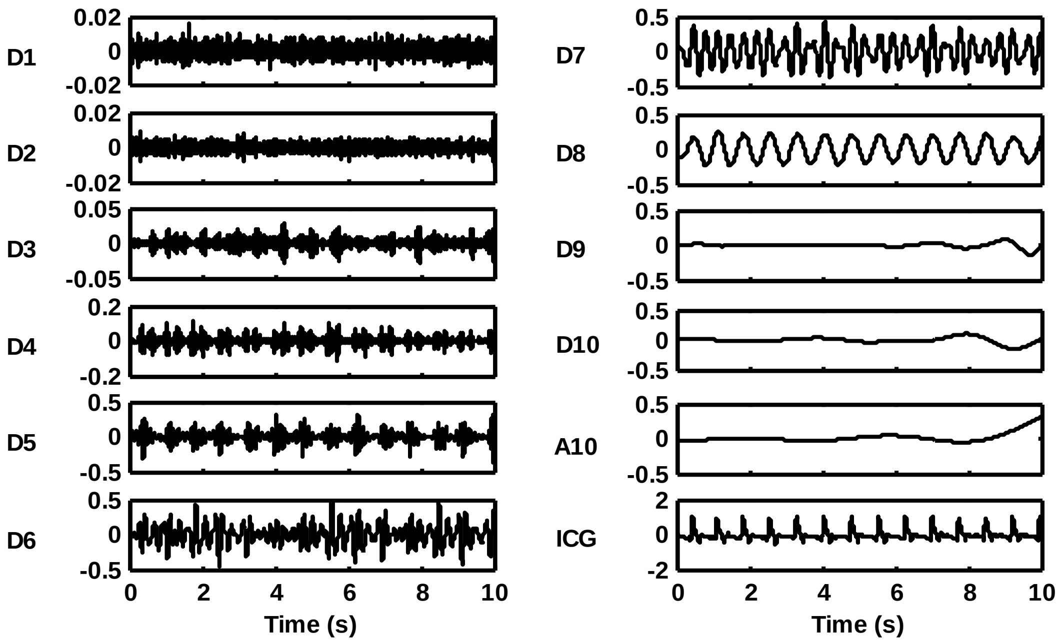

(a) Using dmey wavelet

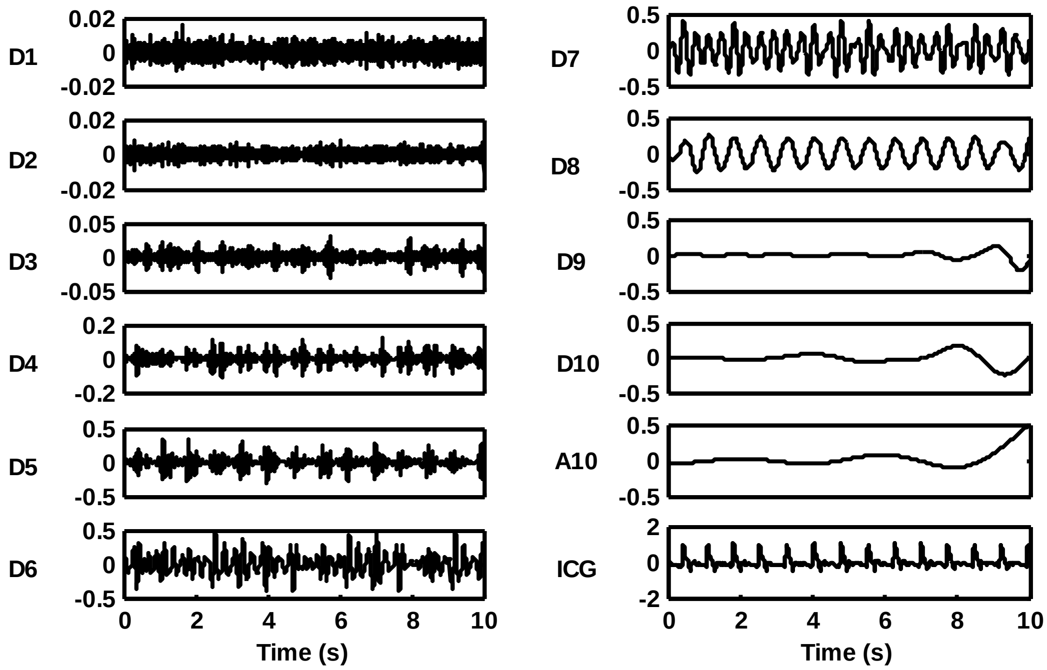

(b) Using sym26 wavelet

Fig. 3.1 Details D1-D10 and approximation A10 of an artifact-free ICG signal, using (a) dmey and (b) sym26 wavelets. (All the waveforms are in arbitrary units).

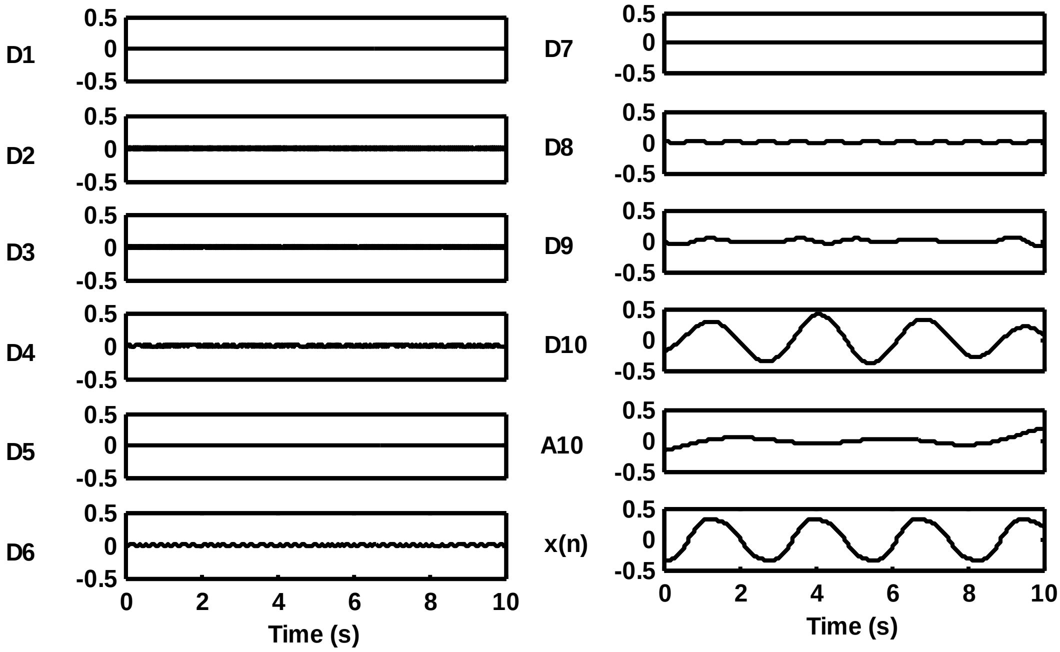

(a) Using dmey wavelet

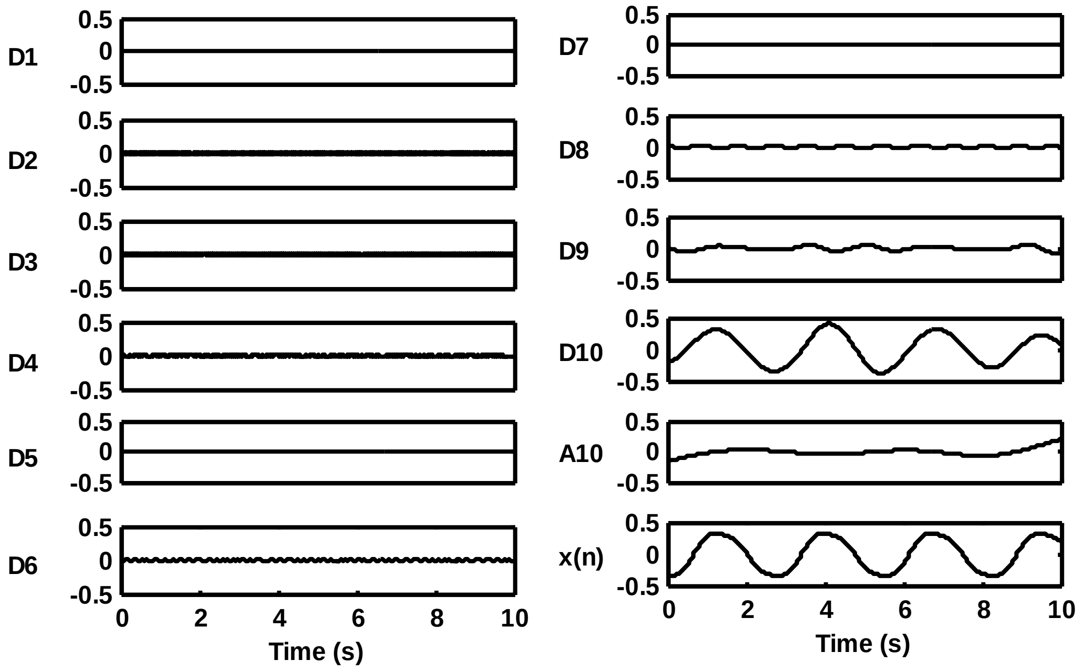

(b) Using sym26 wavelet

Fig. 3.2 Details D1-D10 and approximation A10 of an ICG-free artifact, using (a) dmey and (b) sym26 wavelets. (All the waveforms are in arbitrary units).

Table 3.1 The RMS error in reconstructing an artifact-free ICG signal using first *n* details

Reconstruction	RMS error (%)				
	dmey	sym26	coif5	db8	bior4.4
d1	99	99	99	99	99
d1+d2	99	99	99	99	99
d1+d2+d3	98	98	97	98	97
d1+…+d4	91	91	90	89	90
d1+…+d5	70	70	71	71	68
d1+…+d6	40	40	40	40	41
d1+…+d7	14	14	14	14	15
d1+…+d8	1	1	2	2	2
d1+…+d9	0	0	0	0	0
d1+…+d10	0	0	0	0	0
d1+…+d10+a10	0	0	0	0	0

The m^{th} level partial reconstruction $\hat{x}_m(n)$ was obtained as

$$\hat{x}_m(n) = \sum_{i=1}^{m} d_i(n) \tag{3.5}$$

The RMS error between $\hat{x}_m(n)$ and $x(n)$ were obtained and the RMS errors are given in Table 3.1. It can be seen that both dmey and sym26 are equally effective in capturing the ICG components in the first eight details and the artifact components in the remaining details. The average RMS error in reconstructing the artifact-free ICG from the first eight scales, for 29 artifact-free ICG segments of 10 s duration each, was found to be 1.5% for both the wavelets. The RMS error in reconstructing an ICG-free artifact is given in Table 3.2. We see that the artifact does not contribute to the first six details. It may be noted that these values can only be taken as indicative because the simulated respiratory artifact is periodic.

Figure 3.3 shows an example of processing of an ICG signal recorded during post-exercise resting state. The ICG signal has no motion artifact, but a large respiratory artifact and high heart rate variability. It is observed that both sym26 and dmey wavelet are effective in suppressing the respiratory artifact. Application of the denoising on a total of 33 ICG recordings from two healthy volunteers gave similar results.

Application of artifact suppression on the set B of signals with simulated respiratory artifacts resulted in almost identical results for both the wavelets. The improvements in SAR achieved by denoising with input SAR in the range -9 to 9 dB are given in Table 3.3. It can be seen that almost similar results are obtained with dmey and sym26 wavelets. The corresponding values of the improvement indices, calculated using (3.3), based on L2 norm and max-min are given in Table 3.4.Improvement indices of values close to 1 are achieved at input SAR of -9, -3, and 3 dB which indicates an effective denoising without any significant signal distortion.

Table 3.2 The RMS error in reconstructing an ICG-free artifact using first *n* details

Reconstruction	RMS error (%)				
	dmey	sym26	coif5	db8	bior4.4
d1	100	100	100	100	100
d1+d2	100	100	100	100	100
d1+d2+d3	100	100	100	100	100
d1+…+d4	100	100	100	100	100
d1+…+d5	100	100	100	100	100
d1+…+d6	100	100	100	100	100
d1+…+d7	99	99	99	99	99
d1+…+d8	98	98	97	98	96
d1+…+d9	85	82	76	74	71
d1+…+d10	35	35	35	35	34
d1+…+d10+a10	0	0	0	0	0

Table 3.3 SAR improvement in dB for ICG signals with simulated respiratory artifacts.

Wavelet	Input SNR (dB)			
	-9	-3	3	9
Dmey	23.5	19.6	15.0	9.9
sym26	23.6	19.6	15.1	10.0

Table 3.4 Improvement indices of L2 norm (and max-min) for ICG signals with simulated respiratory artifacts.

Wavelet	Input SNR (dB)			
	-9	-3	3	9
dmey	1.0 (1.0)	1.0 (1.0)	1.1 (1.2)	1.4 (2.9)
sym26	1.0 (1.0)	1.0 (1.0)	1.1 (1.2)	1.5 (2.1)

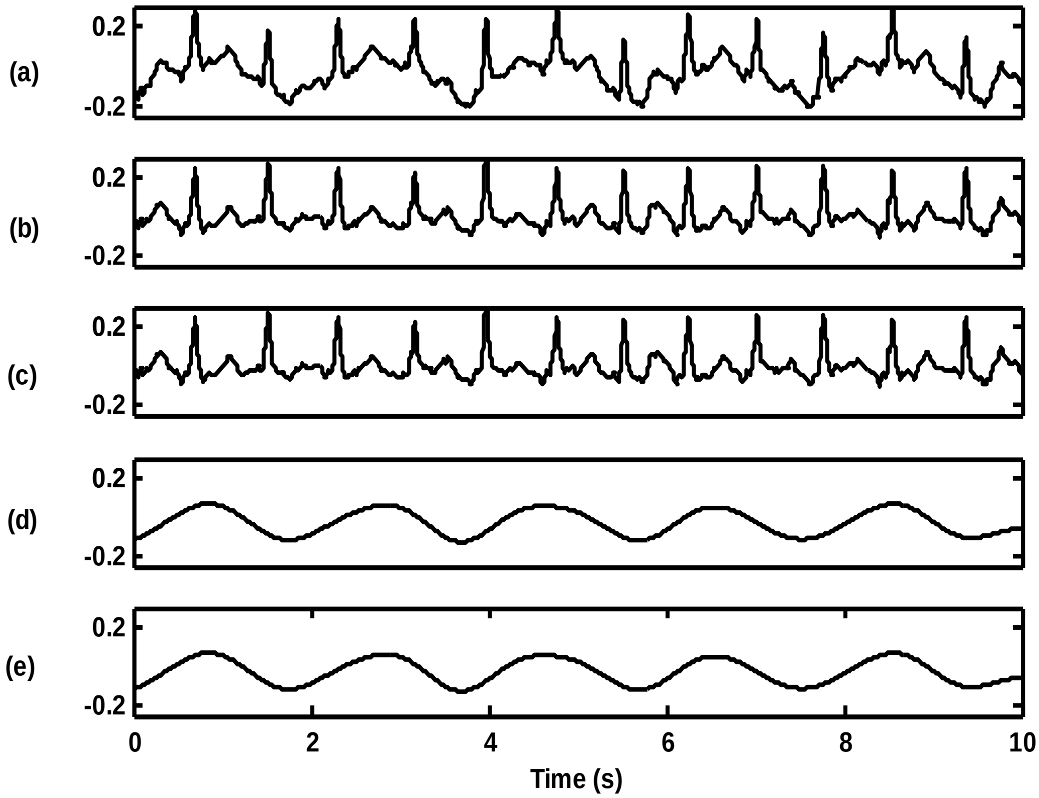

Fig. 3.3 Processing of an ICG signal for the suppression of respiratory artifact: (a) recorded ICG, (b) denoised ICG using dmey wavelet, (c) denoised ICG using sym26 wavelet, (d) recovered respiratory artifact using dmey wavelet, and (e) recovered respiratory artifact using sym26 wavelet, All waveforms are in in Ω/s.

Figure 3.4 shows an example of processing of one of the signals in set A, with ICG contaminated by respiratory and motion artifacts. The signal was recorded during a mild level of physical activity involving hand movement and no restriction on respiration. After denoising for suppressing respiratory artifact, denoising using wavelet coefficient limiting was applied. The recovered signal is found to be almost free of both the artifacts. The wavelet coefficients of the details D1–D5 of the ICG signal given in Fig. 3.4 are given in Fig 3.5. It can be seen that during segments with the motion artifacts, the coefficients achieve relatively higher values and are easily distinguishable from those representing the signal components Application of the denoising technique on several 10 s segments taken from each of two subjects and a qualitative assessment of the processed outputs showed that the technique was able to effectively suppress the artifacts. Application of the technique on artifact-free segments did not introduce any visible signal distortion. An example of the application of the denoising techniques on an ICG signal recorded with no voluntary motion is given Fig. 3.8. It can be seen that application of the technique does not introduce any visible distortion to the signal.

A quantitative evaluation of denoising of recordings with actual respiratory artifact and combination of motion and respiratory artifacts was carried out by applying the technique on the set A of signals and by computing the improvement indices using manually selected artifact-free segments as the reference. The average for both the indices was 1.02, indicating that artifacts were suppressed without introducing any significant distortion in the signal.

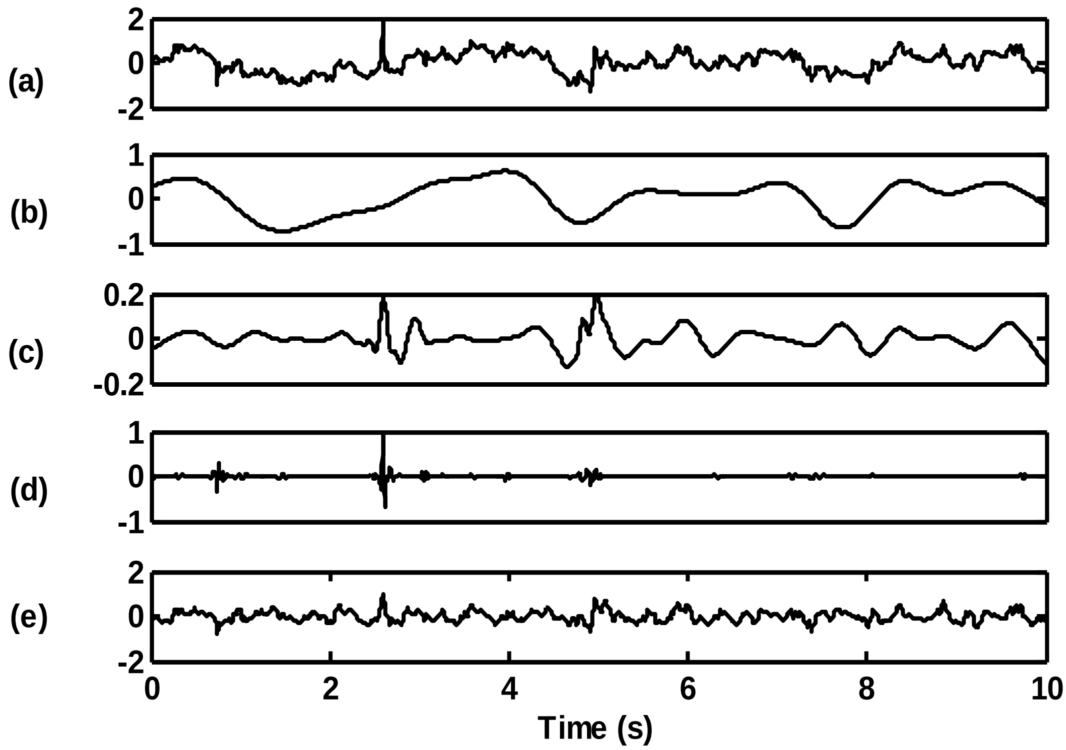

Fig. 3.4 Example of processing of an ICG signal with respiratory and motion artifacts. (a) recorded ICG, (b) recovered respiratory artifact, (c) recovered motion artifact (D5–D8), (d) recovered motion artifact (D1–D5), and (e) denoised ICG, all waveforms are in in Ω/s.

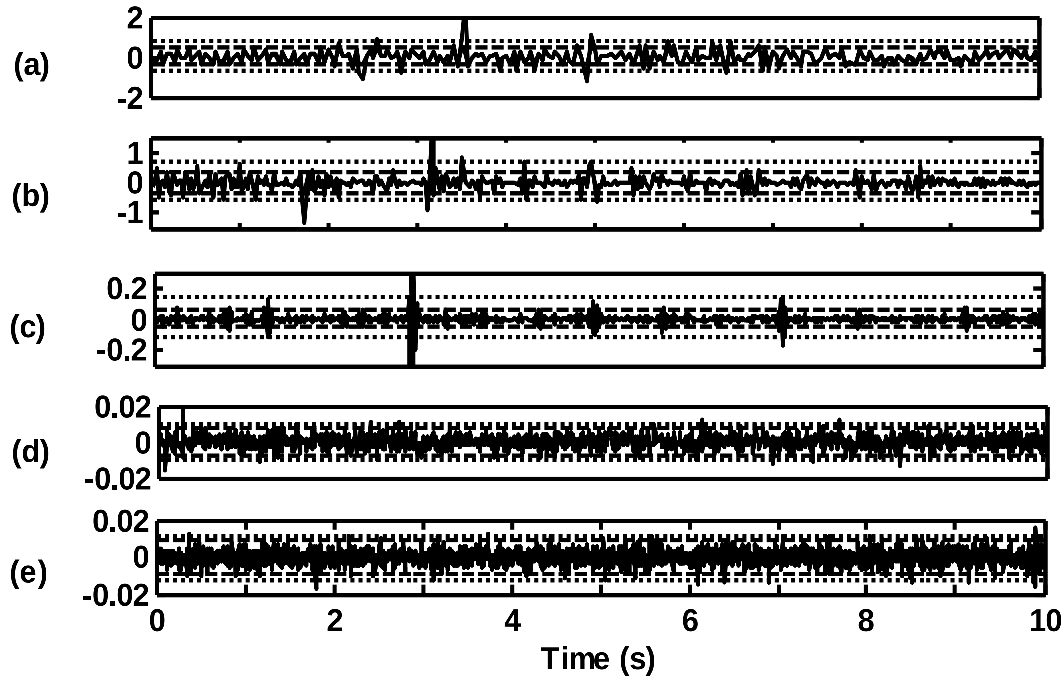

Fig. 3.5 Wavelet coefficients of the details D5 (a) through D1 (e) of the ICG signal given in Fig 3.6. The spike in the coefficients indicates presence of strong motion artifact.

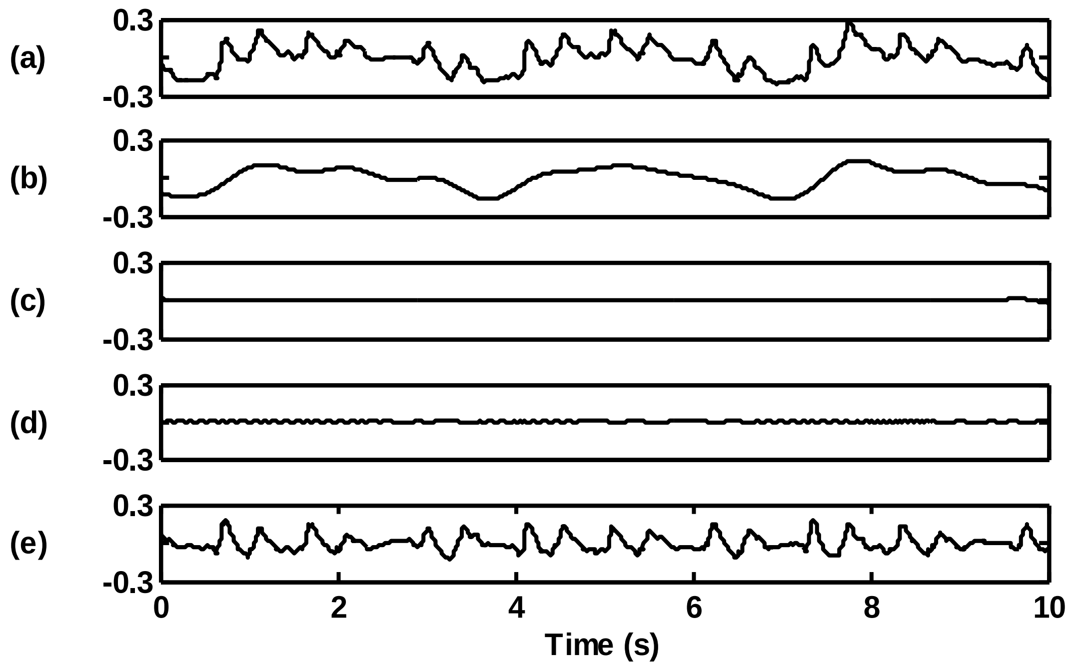

Fig. 3.6 Example of processing of an ICG signal with no voluntary motion artifacts. (a) recorded ICG, (b) recovered respiratory artifact, (c) recovered motion artifact (D5–D8), (d) recovered motion artifact (D1–D5), and (e) denoised ICG, all waveforms are in in Ω/s.

3.5 Discussion

Wavelet based decomposition of artifact-free ICG signals and simulated signal-free respiratory artifact showed that use of sym26 and dmey wavelets resulted in a more compact representations as compared to the other wavelets, with the signal being represented in the lower details and the respiratory artifact being represented in higher details.

The investigated technique uses scale-dependent thresholding for suppression of respiratory artifact and wavelet coefficient limiting for suppression of motion artifact. Denoising of ICG signals with simulated respiratory artifacts of -9 dB resulted in an SAR improvement of 23.5 dB. At this input SAR, the improvement indices were close to one, indicating significant artifact suppression without any significant signal distortion. Denoising of ICG recordings with actual respiratory and motion artifacts resulted in improvement indices of values close to one, indicating that artifacts were suppressed without introducing any significant distortion in the signal. Quantitative and qualitative assessment of the technique by applying it on recordings from several healthy subjects showed that both types of artifacts were suppressed without introducing any visible signal distortion.

The results of denoising showed that dmey and sym26 were almost equally effective. As the filter lengths of sym26 and dmey are 52 and 102, respectively, sym26 should be preferred as its use will involve less computation.

The techniques need to be further validated on recordings from healthy subjects and patients in a clinical setting, and the estimation of the stroke volume estimated by impedance cardiography needs to be compared with the values obtained by established techniques like Doppler echocardiography. The denoising technique may be useful in processing of the ICG signals for beat-to-beat estimation of cardiovascular indices without placing restrictions on respiration and motion. It may help in extending the application of impedance cardiography to ambulatory and stress test recordings.

Chapter 4
WAVELET BASED DENOISING OF ECG

4.1 Introduction

This chapter presents a wavelet based technique for the denoising of ECG signals. It does not require a reference signal and it can be applied on a single-channel recording. EMG noise is reduced by thresholding the wavelet coefficients using an improved thresholding function combining the features of hard and soft thresholding [43]. Motion artifact is reduced by limiting the wavelet coefficients. Thresholds for both the denoising steps are estimated using the statistics of the noisy signal. All the analysis and processing were carried out using Matlab. The denoising technique, method of evaluation, and results are described in the following sections.

4.2 Denoising of ECG

Several wavelet bases, *e.g.* Daubechies (db4, db8), symlets (sym4, sym7, sym8, sym10), Coiflets (coif5), dmey, and biorthogonal (bior4.4), have been used for ECG denoising [35]. The denoising is effective if the dilated version of the wavelet (or the scaling function) at some scale matches the shape of the signal or noise components. In ECG, the baseline wander and motion artifact components do not have a characteristic shape and all the above wavelet bases show a similarity with the ECG signal components at some scale. Mithun [24] has reported a study for the selection of wavelet basis to be used in the suppression of motion artifact and baseline wander in ECG signals. Several wavelets like db8, dmey, sym10, and bior6.8 were investigated for the decomposition and subsequent denoising of the ECG signal. These wavelets and the associated scaling functions are shown in Fig. A.1 in Appendix A. Based on quantitative and qualitative evaluations like visual evaluation of signal enhancement, SNR improvement, and improvement in R-peak detection using automated R-peak detection, best results were reported for dmey wavelet compared to the other wavelets. Hence we have used dmey for our investigation [43]. The slow baseline wander was suppressed by setting A_{10} to zero. The EMG noise and motion artifact were suppressed using non-linear modifications of the wavelet coefficients as described in the following two subsections.

4.2.1 Suppression of EMG Noise

EMG noise is a non-stationary broadband noise. In ECG recordings with 360 Hz sampling, it gets predominantly represented in the initial four details and particularly in D_1, as indicated by a high average absolute value of D_1 in segments with significant EMG noise. For suppressing the EMG noise, a thresholding operation is applied on the wavelet coefficients. For each scale i, a time-varying threshold $\theta_i(n)$ is obtained by scaling the span of the coefficients as obtained from the long-term statistics of the noisy signal with a scaling factor $\gamma(n)$ obtained from a short-time estimate of the level of the EMG noise in the signal. For robustness against excessive noise in some segments, the 90th percentile of the coefficients is taken as the span, and the threshold is given as

$$\theta_i(n) = \gamma(n)\ \text{p90}\left[\,|D_i(n)|\,\right] \tag{4.1}$$

A moving-window average of absolute value of D_1, avgD1(n), is used as the short-time estimate of the level of the EMG noise. A 35-point window is used as it approximates the duration of typical short bursts of EMG noise. Its 5-percentile is taken as a lower threshold avgD1L and half of its 95-percentile is taken as the upper threshold avgD1H. These thresholds are used for thresholding, limiting, and normalizing the short-time average to get the time varying scaling factor

$$\gamma(n) = \begin{cases} 0, & \text{avgD1}(n) < \text{avgD1L} \\ \dfrac{\text{avgD1}(n) - \text{avgD1L}}{\text{avgD1H} - \text{avgD1L}}, & \text{avgD1L} \le \text{avgD1}(n) \le \text{avgD1H} \\ 1, & \text{avgD1}(n) > \text{avgD1H} \end{cases} \tag{4.2}$$

As D_1 has insignificant contribution from ECG, it is totally removed. Before using it for thresholding, $\theta_i(n)$ is resampled to match its number of points to that in D_i.

As D_2–D_4 have significant contributions from the signal as well as from EMG noise, hard thresholding may introduce significant signal distortion and soft thresholding may not effectively suppress the artifact. Hence D_2–D_4 are modified by using an improved thresholding function, combining the features of hard thresholding and soft thresholding as

$$\hat{D}_i(n) = \begin{cases} 0, & |D_i(n)| < \theta_i(n) \\ \operatorname{sgn}\left(D_i(n)\right)\left(|D_i(n)| - f(n)\right), & \theta_i(n) \le |D_i(n)| \le \theta_i(n) + S_i/2 \\ \operatorname{sgn}\left(D_i(n)\right)\left(|D_i(n)| - g(n)\right), & \theta_i(n) + S_i/2 < |D_i(n)| < \theta_i(n) + S_i \\ D_i(n), & \theta_i(n) + S_i \le |D_i(n)| \end{cases} \tag{4.3}$$

where

$$\begin{gathered} f(n) = \theta_i(n)\left[1 - 0.5(e^{ar} - 1)/(e^{a} - 1)\right], \\ r = (|D_i(n)| - \theta_i(n))/(S_i/2) \end{gathered} \tag{4.4}$$

$$\begin{gathered} g(n) = \theta_i(n)\left[0.5 - 0.5(1 - e^{-ar})/(1 - e^{-a})\right], \\ r = (|D_i(n)| - \theta_i(n) - S_i/2)/(S_i/2) \end{gathered} \tag{4.5}$$

The factor a controls the transition between soft and hard thresholding. Setting $a \approx 3$ and the transition span, S_i, as

$$S_i = 0.75 \text{ p95}[\,|D_i(n)|, \quad |D_i(n)| > \theta_i(n)] \tag{4.6}$$

results in a thresholding which combines the features of hard and soft thresholding without showing disadvantages of either of them. The smoothness of the curve is determined by the constant a. We are also investigating the use of another thresholding function with a sinusoidal transition from lower to upper threshold and given as,

$$\hat{D}_i(n) = \begin{cases} 0, & |D_i(n)| < \theta_i(n) \\ \dfrac{D_i(n)}{2}\left[1 - \cos\left(\dfrac{(|D_i(n)| - \theta_i(n))\pi}{S_i}\right)\right], & \theta_i(n) \le |D_i(n)| \le \theta_i(n) + S_i \\ D_i(n), & |D_i(n)| > \theta_i(n) + S_i \end{cases} \tag{4.7}$$

A plot of the hard thresholding, the soft thresholding and the two improved thresholding functions are given in Fig. 4.1.

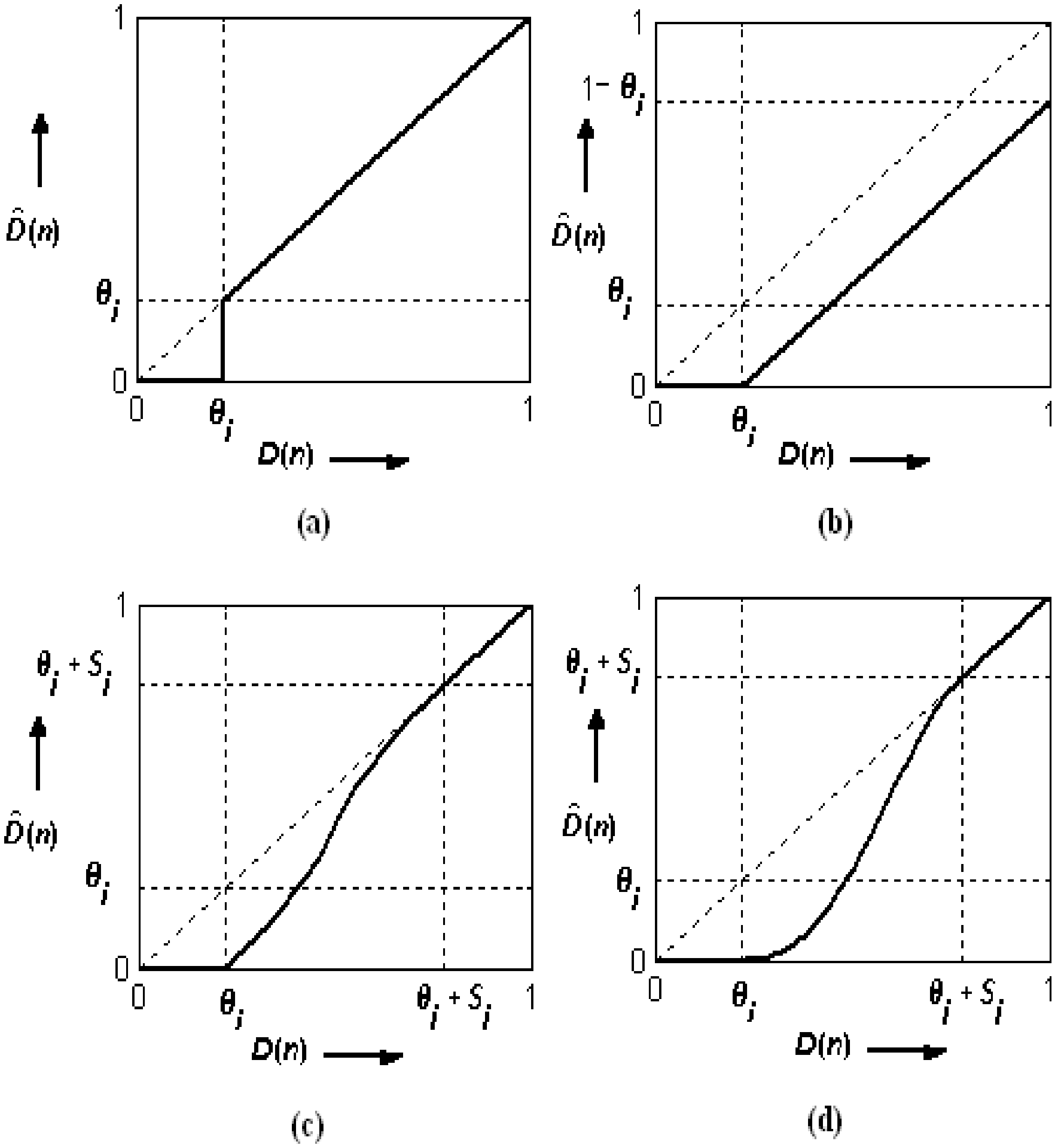

Fig 4.1. Thresholding: (a) hard thresholfing, (b) soft thresholding, (c) thresholding function as given in Eq. 4.3 with a = 3, (d) thresholding function as given in Eq. 4.7

Thresholding generally introduces discontinuities in the wavelet coefficients, which may results in oscillations due to Gibbs phenomenon at the sharp discontinuities in the reconstructed signal. If the discontinuity occurs at the quickly varying portion of the wavelet representing that region, the oscillation will have low amplitude. If the location of discontinuity is at a smooth portion of the wavelet, a high oscillation will result. A method called translation invariant denoising (TI denoising) [28], [29] with one sample shift and 125 iterations is implemented to suppress the oscillations due to Gibbs phenomenon.

4.2.2 Suppression of Motion Artifact

Most of the noise suppression techniques using wavelet thresholding are based on the assumption that the noise is always present and has low amplitude, and that the signal is present in specific time segments and has relatively high amplitude [41]. In ECG corrupted with non-stationary motion artifact, ECG signal is always present and the motion artifact occurs intermittently and it generally has high amplitude. Hence limiting of the wavelet coefficients is investigated for suppressing the motion artifact. The limiting operation, using threshold ϕ_i, on $D_i(n)$ is carried out as

$$\hat{D}_i(n) = \begin{cases} D_i(n), & |D_i(n)| \le \phi_i \\ \operatorname{sgn}\left(D_i(n)\right)\phi_i, & |D_i(n)| > \phi_i \end{cases} \tag{4.8}$$

The threshold ϕ_i is an estimate of the maximum value of the wavelet coefficients of the ECG signals at scale *i*. It should be high enough to exclude the possibility of reducing the coefficients representing noise-free ECG, and low enough to significantly suppress the motion artifact. The thresholds are estimated by dividing the ECG record into segments of two average cardiac cycles. At each scale *i*, the maximum absolute values of coefficients in these segments are used to calculate the average μ_i and standard deviation σ_i. The limiting threshold for scale *i* is calculated as $\phi_i = \mu_i - \eta\sigma_i$, a value of η close to 0.1 resulted in effective denoising without causing signal distortion, while a larger value caused distortion in artifact-free ECG segments.

The coefficient limiting, given by Eq. 4.8, is a hard-limiting operation as shown in Fig. 4.2 (a). The values below the threshold ϕ_i are unaffected and those above it are limited to ϕ_i. In addition to the hard-limiting, soft-limiting using several functions was also investigated. It involves using two additional threshold values ϕ_i' and ϕ_i'' on either side of ϕ_i. The coefficients below the threshold ϕ_i' remain unmodified, while the coefficients above ϕ_i'' are limited to ϕ_i. The coefficients lying between the thresholds ϕ_i' and ϕ_i'' are modified using a function having a transition from ϕ_i' to ϕ_i. One such function is a piecewise linear function, shown in Fig. 4.2 (b), and given as

$$\hat{D}_i(n) = \begin{cases} D_i(n), & |D_i(n)| < \phi_i' \\ \operatorname{sgn}\left(D_i(n)\right)\left(\phi_i' + \dfrac{\phi_i - \phi_i'}{\phi_i'' - \phi_i'}\left(|D_i(n)| - \phi_i'\right)\right), & \phi_i' \leq |D_i(n)| \leq \phi_i'' \\ \operatorname{sgn}\left(D_i(n)\right)\phi_i, & \phi_i'' < |D_i(n)| \end{cases} \quad (4.9)$$

A soft-limiting function with a sinusoidal transition is given as the following

$$\hat{D}_i(n) = \begin{cases} D_i(n), & |D_i(n)| < \phi_i' \\ \operatorname{sgn}\left(D_i(n)\right)\left(\phi_i' + \left(\phi_i - \phi_i'\right)\sin\left(\dfrac{\left(|D_i(n)| - \phi_i'\right)\pi/2}{\left(\phi_i'' - \phi_i'\right)}\right)\right), & \phi_i' \leq |D_i(n)| \leq \phi_i'' \\ \operatorname{sgn}\left(D_i(n)\right)\phi_i, & \phi_i'' < |D_i(n)| \end{cases}$$

(4.10)

where $(\phi_i - \phi_i')/(\phi_i'' - \phi_i) = 2/\pi$. The function and its derivative both are continuous, as shown in Fig 4.2 (c). A soft-limiting function with a parabolic transition from the lower threshold ϕ_i' to the upper threshold ϕ_i'' is given as

$$\hat{D}_i(n) = \begin{cases} D_i(n), & |D_i(n)| < \phi_i' \\ \operatorname{sgn}\left(D_i(n)\right)\left(\phi_i - \left(\dfrac{\left(\phi_i'' - |D_i(n)|\right)^2}{2\left(\phi_i'' - \phi_i'\right)}\right)\right), & \phi_i' \leq |D_i(n)| \leq \phi_i'' \\ \operatorname{sgn}\left(D_i(n)\right)\phi_i, & \phi_i'' < |D_i(n)| \end{cases} \quad (4.11)$$

where $\phi_i = (\phi_i' + \phi_i'')/2$. The function and its derivative are continuous as shown in Fig. 4.2(d).

4.3 Method of Evaluation

Performance of the denoising techniques has been generally reported in the form of SNR improvement for ECG inputs obtained by adding different levels and types of noise to noise-free ECG [7], [8], [29], [34], [35]. For real ECG records, noise reduction is generally assessed by visual inspection [13], [28], [33]. Tong *et al.* [7] used improvement indices (as given earlier in Eq. 3.3) based on signal excursion (max-min) and L_2 norm to quantify the ECG enhancement in real ECG records.

The denoising was carried out by applying EMG noise reduction followed by motion artifact reduction. The technique was evaluated by applying it on simulated noisy ECG records and on ambulatory ECG records. The simulated noisy records were obtained by adding ECG records from the MIT/BIH arrhythmia database [38] and ECG-free noise records from the MIT/BIH noise stress test database [39], having waveforms with 360 Hz sampling rate and 11-bit resolution. From each of the 48 two-channel ECG records in the database, single channel ECG signals of one min. duration were taken as noise-free ECG. Segments from the EMG noise ("ma") and motion artifact ("em") were taken as the noise. All the records were scaled to have the same RMS value. Simulated noisy records with different values of SNR were generated by scaling the noise and adding it to the signal. The noises used were EMG noise, motion artifact, and a mix of EMG noise and motion artifact in 1:2 ratio (approximating the occurrence in ambulatory recordings). Ambulatory ECG signals were recorded using a Holter monitor (ECIL, Hyderabad, India) at 200 Hz with 8-bit resolution. The recordings were resampled to 360 Hz (the sampling rate used in the MIT/BIH database). The recordings were taken from five healthy volunteers in resting condition and during common ambulatory activities like hand movements, walking, and climbing stairs.

A qualitative evaluation of the denoising on both types of records involved a visual examination of the output for suppression of the artifact and presence of distortion. A quantitative evaluation involved calculation of improvement in the SNR for the simulated noisy records. Another quantitative evaluation, as used by Tong et al. [7], involved the improvement indices (II) based on L2 norm and excursion (max-min) of the signal, and calculated using Eq. 3.3 as given earlier. Improvement in automated R-peak detection using Pan-Tompkins algorithm [11] was also used as a measure of denoising.

Table 4.1 Mean (and std. dev) of SNR improvement (dB) for simulated noisy ECG (No of records = 48)

Noise type	Input SNR (dB)			
	-10	-5	0	5
EMG noise	12.1 (1.7)	8.8 (2.0)	5.1 (2.3)	0.8 (2.6)
Motion artifact	11.5 (0.9)	8.3 (1.4)	4.8 (2.1)	0.7 (2.6)
Mixed	11.4 (0.9)	8.3 (1.5)	4.9 (2.2)	0.7 (2.6)

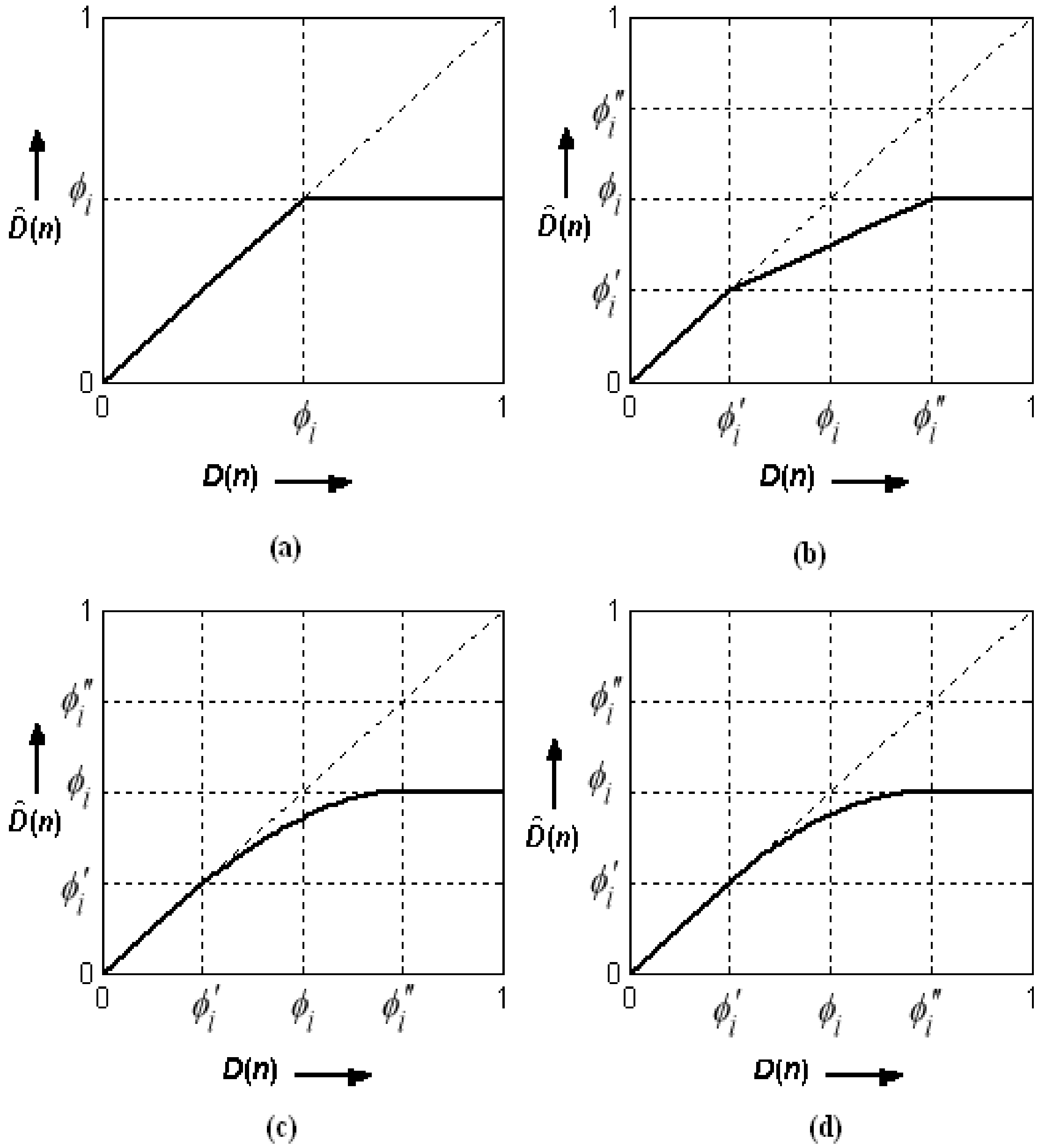

Fig. 4.2 Limiting of wavelet coefficients. (a) hard-limiting, (b) piecewise linear soft-limiting, (c) sinusoidal soft-limiting and (d) parabolic soft-limiting

4.4 Results

The improvements in SNR obtained by denoising are given in Table 4.1. The corresponding improvement indices are given in Table 4.2. The technique was effective in suppressing all the three types of simulated noise, with a mean wander already present in the record. The results of a quantitative evaluation using an automated R-peak detection are given in Table 4.3. Denoising has significantly improved the efficiency of the algorithm. In many of the segments with EMG noise, Gibbs oscillation produced by the thresholding operation, could be observed in the

Table 4.2 Improvement indices of L2 norm (and max-min) for simulated noisy ECG (No of records = 48)

Noise type	Input SNR (dB)			
	-10	-5	0	5
EMG noise	1.0 (1.0)	1.2 (1.2)	1.6 (1.9)	2.8 (11.7)
Motion artifact	1.1 (1.2)	1.2 (1.6)	1.6 (4.2)	2.9 (9.4)
Mixed	1.1 (1.2)	1.2 (1.6)	1.5 (3.9)	2.2 (11.8)

Table 4.3 Rate of success, failures, and false detection in percentage by the automated R-peak detection algorithm for simulated noisy ECG. Total number of cardiac cycles = 407.

Type of ECG record	Success (%)	Failure (%)	False (%)
Pre-denoising	87.0	13.0	1.5
Post-denoising	98.0	2.0	0.2

Table 4.4 Rate of success, failures, and false detection in percentage by the automated R-peak detection algorithm for ambulatory ECG. Total number of cardiac cycles = 551.

Type of ECG record	Success (%)	Failure (%)	False (%)
Pre-denoising	90.2	9.8	2.5
Post-denoising	99.3	0.7	0.7

vicinity of the QRS complexes. Translation-invariant [28], [29] application of the denoising, with 1-sample shift and 125 iterations, reduced these oscillations and resulted in SNR improvement of up to 1 dB.

A visual examination of the processed outputs showed that the denoising technique was effective in suppressing the EMG noise and motion artifact, and it did not result in any visible distortions in the clean segments. The EMG denoising method was found to be effective for the ambulatory recordings. As seen in the example given in Fig. 4.3, the EMG noise present in the ECG record has been attenuated while the EMG-free regions are unaffected. However while the R-peaks outside EMG noise are unaffected, those overlapping with the EMG noise are attenuated (*e.g.*, first R-peak after 6 s in Fig. 4.3.). Another problem observed with the EMG reduction technique was the Gibbs oscillation produced by the thresholding operation. An occurrence of

Gibbs oscillations and its suppression using translation-invariant denoising is shown in Fig. 4.4. It can be seen from Fig. 4.4(c) that use of translation-invariant denoising effectively suppressed the oscillations occurring around the QRS complexes without affecting any of the features in the waveform.

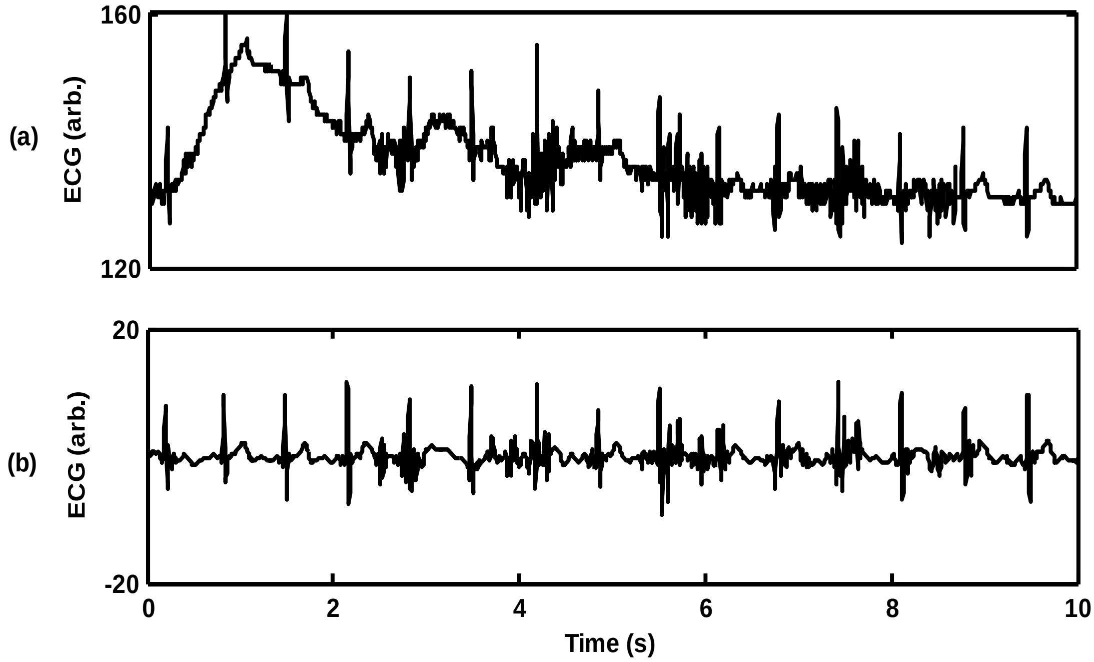

Fig. 4.3 Suppression of EMG noise in ambulatory ECG: (a) Input, (b) Output.

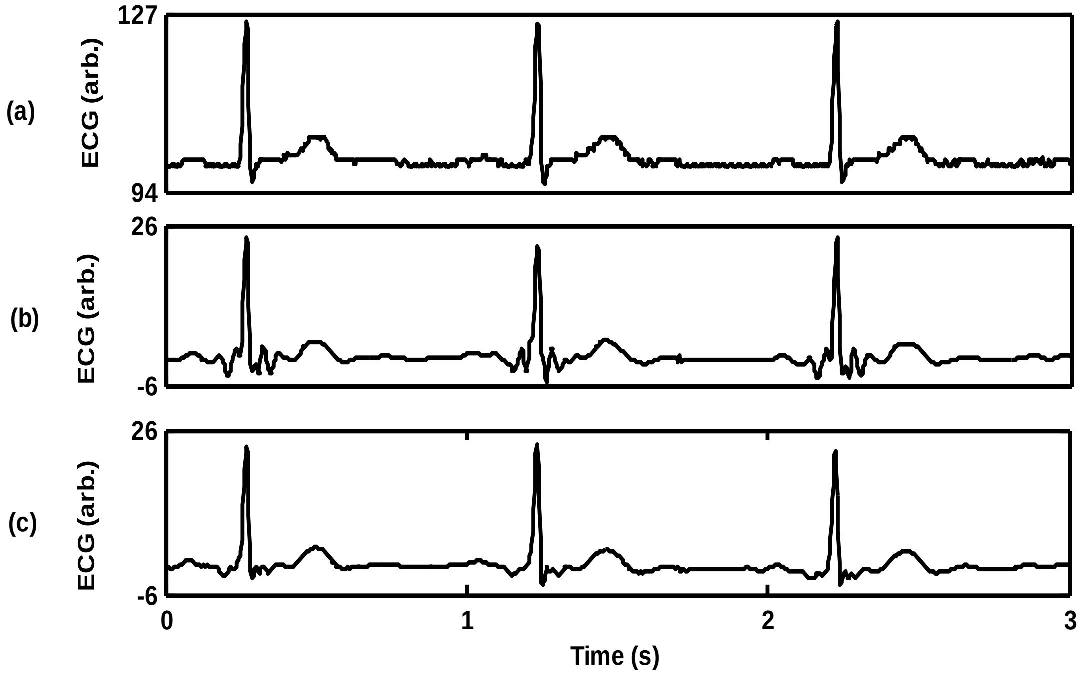

Fig. 4.4 Suppression of Gibbs oscillations in the vicinity of QRS complexes: (a) Input ECG, (b) ECG after EMG denoising, (c) ECG after translation-invariant EMG denoising.

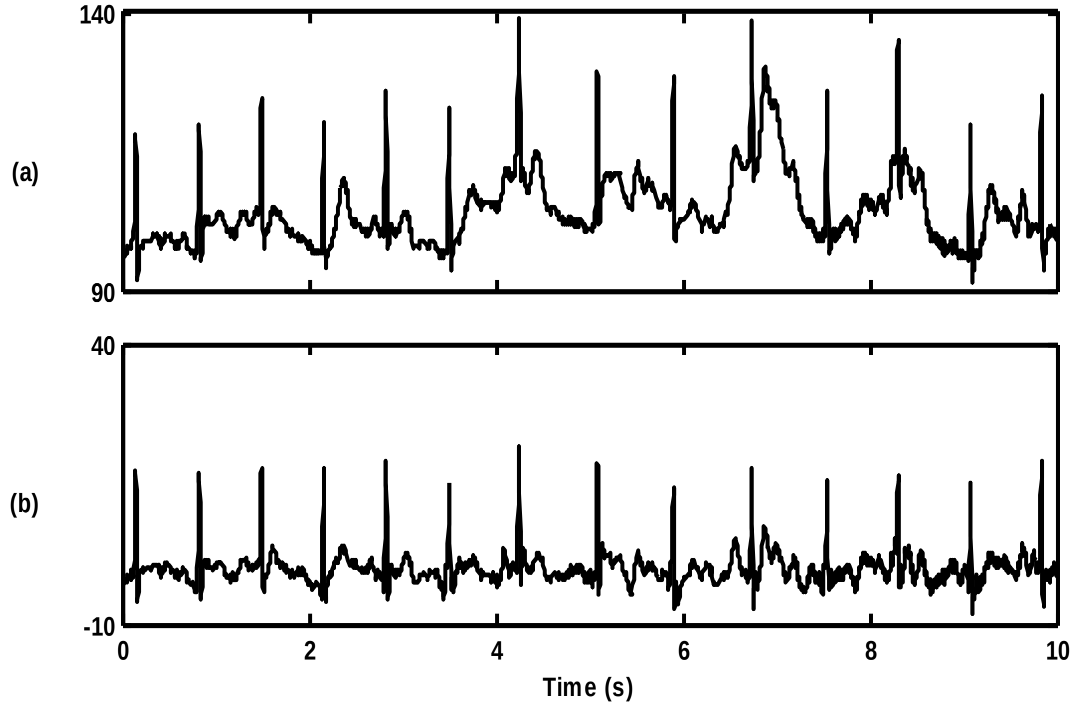

Fig. 4.5 Suppression of motion artifact in ambulatory ECG: (a) Input, (b) Output.

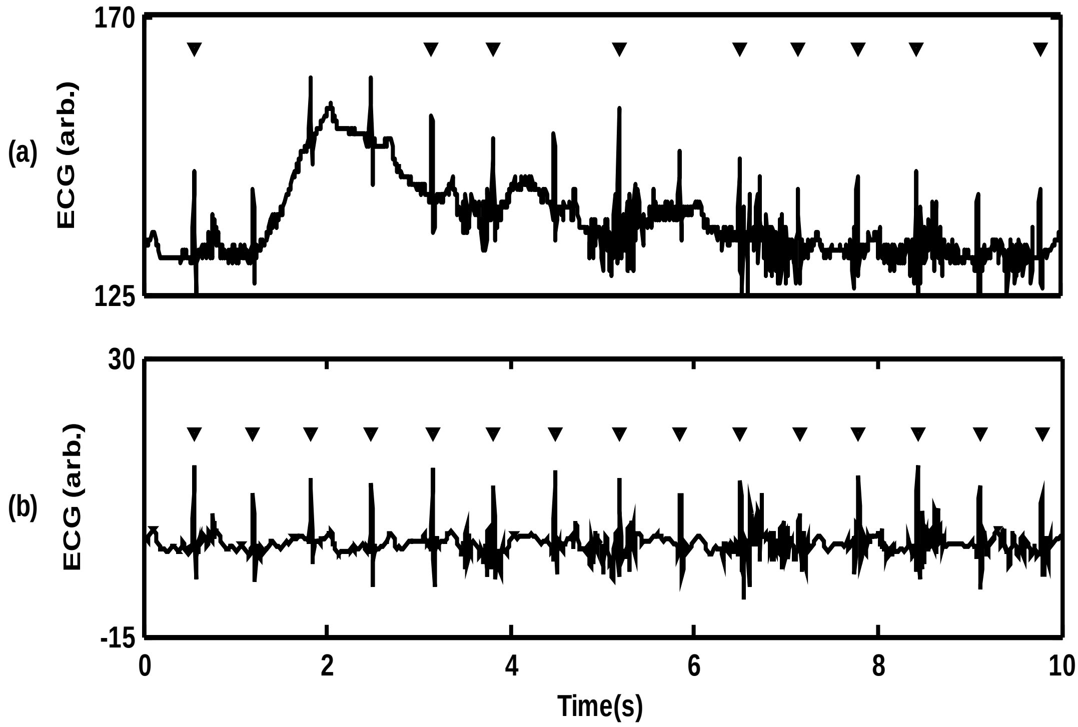

Fig. 4.6 Automated R-peak detection applied on (a) input ECG, (b) ECG after denoising.

A good degree of reduction in motion artifact could be achieved by the wavelet coefficient limiting technique, as seen in the example given in Fig. 4.5. The quickly varying and high amplitude motion artifact seen at the time marked as 6–8 s has been attenuated significantly without attenuating the nearby QRS complexes. It can also be observed that processing did not produce any significant attenuation for the R-peaks in other part of the record where the motion artifact present is very low. Several noise-free ECG segments were processed by the motion-artifact reduction technique, and there were no significant distortions visible in almost all cases.

Another quantitative evaluation of the denoising was in terms of improvement in automated R-peak detection using Pan-Tompkins algorithm [11]. An example of the validation based on the improvement in the R-peak detection peaks from the denoised ECG record, as shown in Fig. 4.6(b). The net rate of successful detections, failures, and false detections for a set of ambulatory ECG records, consisting of 10-s segments from the recordings from five volunteers, different leads, and different ambulatory activities, with a total of 551 cardiac cycles are given in Table 4.4. It shows a large improvement in the efficiency of R-peak detection due to processing, in terms of increase in the successful detection and decrease in the detection failures and false detection.

4.5 Discussion

Wavelet based techniques were investigated for the suppression of EMG noise and motion artifact in ECG. EMG noise was reduced by modified thresholding, combining the features of hard and soft thresholding. Motion artifact was reduced by limiting the wavelet coefficients. Thresholds for both the denoising steps were estimated from the statistics of the noisy signal in an automated manner. Gibbs oscillations due to thresholding, occasionally occurring in the vicinity of QRS complexes, were suppressed by translation-invariant application of denoising. Effectiveness of the technique was qualitatively and quantitatively validated by applying it on simulated noisy ECG records as well as on ambulatory recordings from a Holter recorder. Its application significantly reduced the EMG noise and motion artifact without affecting any of the features in the waveform. Denoising of simulated noisy ECG signals of -10 dB input SNR resulted in an average SNR improvement of 11.4 dB. At this input SNR the improvement indices were close to one, indicating significant artifact suppression without any significant signal distortion. Application of translation-invariant denoising also resulted in an additional SNR improvement of up to 1 dB. Its application on ambulatory ECG recordings resulted in L_2 norm and max-min based improvement indices close to one. Denoising significantly improved the automated R-peak detection in both the cases. Its performance needs to be further evaluated with respect to some of the other techniques and particularly on ECG records from patients with different cardiac disorders.

Chapter 5
SUMMARY AND CONCLUSION

The ECG and ICG are biosignals related to the functioning of the heart. These cardiac biosignals are generally corrupted by artifacts, which may be much stronger than the signal during ambulatory and post-exercise recordings. As the presence of the artifacts may make it difficult to get the desired diagnostic information, it is important to suppress them. Use of wavelet based denoising was investigated for suppressing respiratory and motion artifacts in ICG and for suppressing EMG noise and motion artifact in ECG. It does not need a reference as required in adaptive filter based techniques, multi-channel signals as required by ICA-based techniques, or identification of characteristic points as required in the cubic spline and EMD-based techniques.

It was shown that dmey and sym26 wavelets, as compared to several other wavelets, were better suited for the denoising of ICG. Scale-dependent thresholding was used for the suppression of respiratory artifact in ICG. Motion artifact in ICG was suppressed using wavelet coefficient limiting with the threshold obtained from the statistics of the wavelet coefficients of the noisy signal. Denoising of ICG signals with simulated respiratory artifacts of -9 dB resulted in an SAR improvement of 23.5 dB. At this input SAR, the improvement indices were close to one. Denoising of ICG recordings with actual respiratory and motion artifacts also resulted in improvement indices of values close to one, indicating that artifacts were suppressed without introducing any significant distortion in the signal. Quantitative and qualitative assessment of the technique by applying it on recordings from several healthy subjects showed that both types of artifacts were suppressed without introducing any visible signal distortion.

For wavelet-based denoising of ambulatory ECG, EMG noise was reduced by thresholding, combining the features of hard and soft thresholding. Motion artifact was reduced by limiting the wavelet coefficients. Thresholds for both the denoising steps were estimated from the statistics of the wavelet coefficients of the noisy signal in an automated manner. Gibbs oscillations due to thresholding, occasionally occurring in the vicinity of QRS complexes, were suppressed by translation-invariant application of denoising. Effectiveness of the technique was validated by applying it on simulated noisy ECG records as well as on ambulatory recordings from a Holter recorder. Its application significantly reduced the EMG noise and motion artifact without introducing any visible distortions in ST segments. Denoising of simulated noisy ECG signals resulted in an average SNR improvement of 11.4 dB at -10 dB input SNR, and its application on ambulatory ECG recordings resulted in L_2 norm and max-min based improvement indices close to one. Denoising significantly improved the R-peak detection in both the cases.

Performance of the presented denoising techniques needs to be further validated with respect to some of the other techniques and particularly on records from patients with different cardiac disorders. Denoising techniques for ICG need to be further validated by estimating different cardiovascular indices and comparing with the values obtained by established techniques like Doppler echocardiography. The denoising technique may be useful in processing of the ICG signals for beat-to-beat estimation of cardiovascular indices without placing restrictions on respiration and motion. It may help in extending the application of impedance cardiography to ambulatory and stress test recordings. After such a validation, the proposed techniques may be useful in getting the desired diagnostic information from ambulatory recordings of the ECG and the ICG.

Appendix A

Wavelets and Scaling Functions

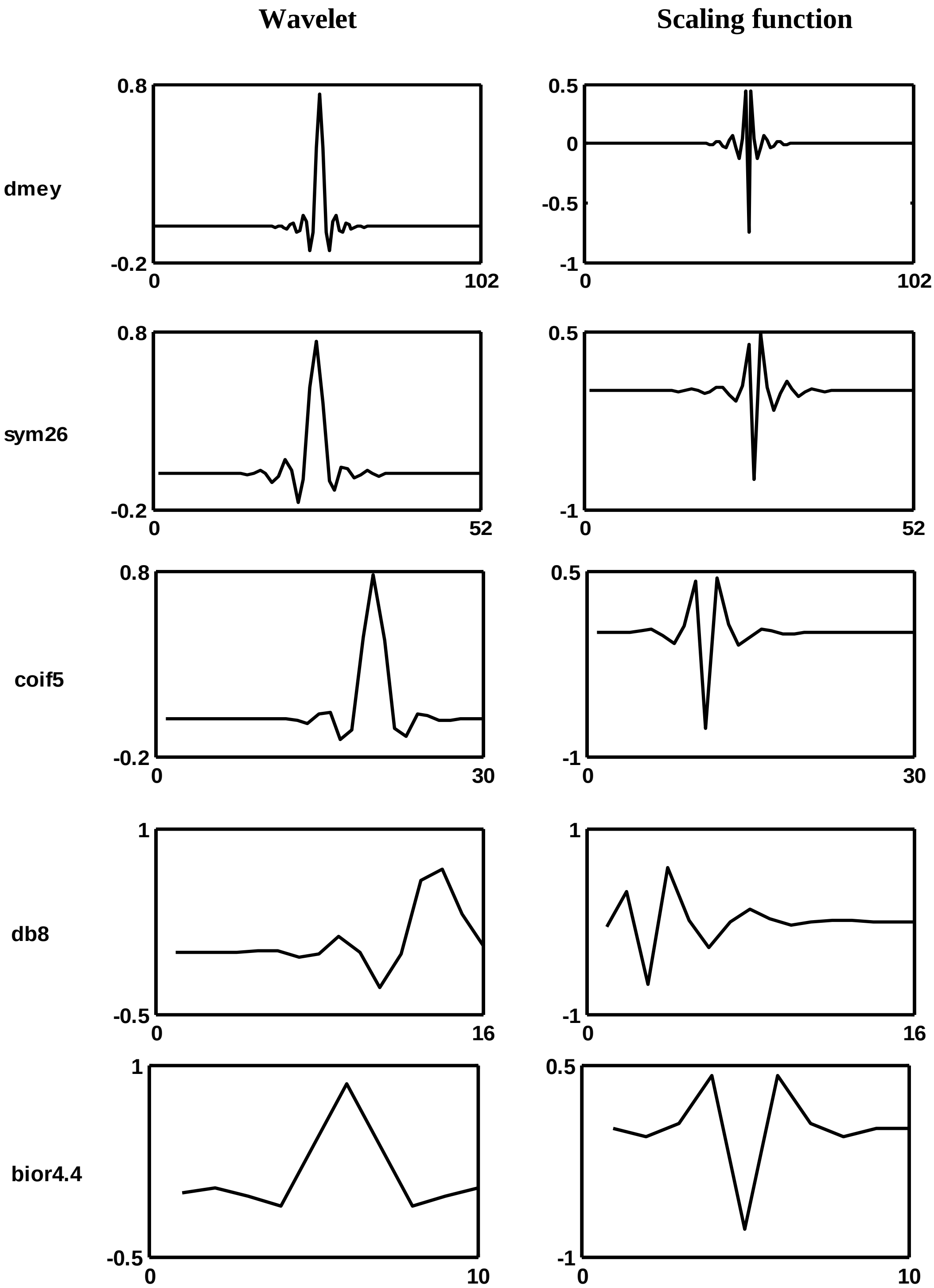

Fig. A.1 Different wavelets and the associated scaling functions used for the study. (x-axis: samples, and y-axis: in arbitrary units.)

REFERENCES

[1] W. G. Kubicek, F. J. Kottke, M. U. Ramos, R. P. Patterson, D. A. Witsor, J. W. Labree, W. Remole, T. E. Layman, H. Schoening, and J. T. Garamela, "The Minnesota impedance cardiograph - theory and application," *Biomed. Eng.*, vol. 9, no. 9, pp. 410 – 417, 1974.

[2] R. P. Patterson, "Fundamentals of impedance cardiography," *IEEE Eng. Med. Biol. Mag.*, vol. 8, no. 1, pp. 35 – 38, 1989.

[3] A. Sherwood, M. T. Allen, J. Fahrenberg, R. M. Kelsey, W. R. Lovallo, and L. J. P. van Doornen "Methodological guidelines for impedance cardiography," *Psychophysiology*, vol. 27, no. 1, pp. 1 – 23, 1990.

[4] A. C. Guyton, *Textbook of Medical Physiology*, 7th ed., Saunders, Philadelphia, PA, 1986.

[5] W. H. Olson, "Basic concepts of medical instrumentation," in *Medical Instrumentation, Application and Design*, J. G. Webster (Editor), Houghton Mifflin, Boston, MA, 1992.

[6] W. J. Tompkins, *Biomedical Digital Signal Processing*, Prentice Hall, New Delhi, 1995.

[7] D. A. Tong, K. A. Bartels, and K. S. Honeyager, "Adaptive reduction of motion artifact in the electrocardiogram," in *Proc. 2nd Joint Conf. EMBS/BMES*, Houston, Texas, 2002, vol. 2, pp. 1403 – 1404.

[8] T. He, G. Clifford, and L. Tarassenko, "Application of ICA in removing artefacts from the ECG," *Neural Comput. and Appl.*, vol. 15, pp. 105 – 116, 2006.

[9] S. V. Pandit, "ECG baseline removal through STFT," in *Proc. 18th Int. Conf. IEEE/EMBS*, Amsterdam, 1996, pp. 1405 – 1406.

[10] M. Dai and S. Lian, "Removal of baseline wander from dynamic electrocardiogram signals," in *Proc. 2nd Int. Congr. Image Sig. Proc.*, Tianjin, China, 2009, pp. 1 – 4.

[11] J. Pan and W. J. Tompkins, "A real-time QRS detection algorithm," *IEEE Trans. Biomed. Eng.*, vol. 32, pp. 230 – 236, 1985

[12] P. S. Hamilton and W. J. Tompkins, "Quantitative investigation of QRS detection rules using the MIT/BIH arrhythmia database," *IEEE Trans. Biomed. Eng.*, vol. 33, pp. 1157 – 1165, 1986.

[13] M. Blanco-Velasco, B. Weng, and K. E. Barner, "ECG signal denoising and baseline wander correction based on the empirical mode decomposition," *Comput. Biol. Med.*, vol. 38, pp. 1 – 13, 2008.

[14] J. A. Van Asté and T. S. Schilder, "Removal of base-line wander and power-line interference from the ECG by an efficient FIR filter with a reduced number of taps," *IEEE Trans. Biomed. Eng.*, vol. 32, pp. 1052 – 1060, 1985.

[15] V. K. Pandey, "Suppression of artifacts in impedance cardiography," *Ph.D Thesis*, Dept. Bioscience and Bioengineering, IIT Bombay, Mumbai, India, 2009.
[16] M. Qu, Y. Zang, J. G. Webster, and W. J. Tompkins, "Motion artifacts from spot and band electrodes during impedance cardiography," *IEEE Trans. Biomed. Eng.*, vol. 33, pp. 1029 – 1036, 1986.
[17] A. K. Barros, M. Yoshiwaza, and Y. Yasuda, "Filtering noncorrelated noise in impedance cardiography," *IEEE Trans. Biomed. Eng.*, vol. 42, no. 3, pp. 324 – 327, 1985.
[18] J. H. Nagel, L. Y. Shylu, S. P. Reddy, B. E. Hurwitz, P. M. McCabe, and N. Schneiderman, "New signal processing techniques for improved precision of noninvasive impedance cardiography," *.Ann. Biomed. Eng.*, vol 17, no. 5, pp. 517 – 534, 1987.
[19] B. E. Hurwitz, L. Y. Shylu, S. P. Reddy, N. Schneiderman, and J. H. Nagel, "Coherent ensemble averaging techniques for impedance cardiography" in *3rd Annu. IEEE Symp. Comp. Based Med. Syst,* Chapel Hill, NC, 1990, pp. 228 – 235.
[20] J Rosell and J. G. Webster, "Signal-to-motion artifacts ratio versus frequency for impedance pneumography," *IEEE Trans. Biomed. Eng.*, vol. 42, no. 3, pp. 321 – 323, 1988.
[21] V. K. Pandey and P. C. Pandey, "Cancellation of respiratory artifacts in impedance cardiography," in *Proc. 27th Annl. Int. Conf. IEEE/EMBC*, Shanghai, Chaina, 2005, pp. 191 – 194.
[22] Y. Yamamoto, K. Mokushi, S. Tamura, Y. Mutoh, M. Miyashita, and H. Hamamoto, "Design and implementation of a digital filter for beat-by-beat impedance cardiography," *IEEE Trans. Biomed. Eng.,* vol. 35, no. 12, pp. 1086 – 1090, 1988.
[23] S. B. Raza, R. P. Patterson, and L. Wang "Filtering respiration and low-frequency movement artefacts from the cardiogenic electrical impedance signal," *Med. Biol. Eng. Comput.*, vol. 30, no. 5, pp. 556-561, 1992.
[24] P. Mithun, "ECG baseline wander correction and noise reduction," *M. Tech Dissertation*, Dept. Bioscience and Bioengineering, IIT Bombay, Mumbai, India, 2010.
[25] Y. Zhang, M. Qu, J. G. Webster, W. J. Tompkins, B. A. Ward, and D. R. Bassett, "Cardiac output monitering by impedance cardiography during threadmill exercise," *IEEE Trans. Biomed. Eng.*, vol. 33, pp. 1037 – 1041, 1986.
[26] H. Riese, P. F. C. Groot, M. V. D. Berg, N. H. M. Kupper, E. H. B. Magnee, and E. J. Rohaan "Large-scale ensemble averaging of ambulatory impedance cardiograms," *Behavior Research Methods, Instruments, & Computers,* vol. 35, vol. 3, pp. 467 – 477, 2003.
[27] V. K. Pandey and P. C. Pandey "Cancellation of respiratory artifact in impedance cardiography," in *Proc. 27th Ann. Int. Conf. IEEE Eng. Med. Biol. Soc.*, 2005, pp. 3486 – 3489.
[28] D. Zhang, "Wavelet approach for ECG baseline wander correction and noise reduction," in *Proc. 27th Int. Conf. IEEE/EMBS*, Shanghai, China, 2005, pp. 1212 – 1215.
[29] L. Su and G. Zhao, "De-noising of ECG signal using translation-invariant wavelet de-noising method with improved thresholding," in *Proc. 27th Int. Conf. IEEE/EMBS*, Shanghai, China, 2005, pp. 5946 – 5949.

[30] S. Guoxiang and Z. Ruizhen, "Three novel models of threshold estimator for wavelet coefficients," in *Lecture Notes in Computer Science: Wavelet Analysis and Its Applications*, Y. Y. Tang *et al.*, Eds, Berlin: Springer-Verlag, vol. 2251, pp. 145 – 150, 2001.

[31] J. Ouyang, X. Gao, and Y. Zhang "Wavelet-based method for reducing respiratory interference in thoracic electrical bioimpedance," in *Proc. 20th Ann. Int. Conf. IEEE Eng. Med. Biol. Soc*., 1998, pp. 1446 – 1449.

[32] M. Jansen, "Wavelet thresholding and noise reduction," *Ph.D Thesis*, Dept. Comp. Sci., Katholieke Universiteit, Leuven, Belgium, 2000.

[33] V. Cherkassky and S. Kilts, "Myopotential denoising of ECG signals using wavelet thresholding methods," *Neural Networks*, vol. 14, no. 8, pp. 1129 – 1137, 2001.

[34] B. N. Singh and A. K. Tiwari, "Optimal selection of wavelet basis function applied to ECG signal denoising," *Dig. Sig. Proc.*, vol. 16, no. 3, pp. 275 – 287, 2006.

[35] S. Li and J. Lin, "The optimal de-noising algorithm for ECG using stationary wavelet transform," in *Proc. 2009 WRI World Cong. Computer Science Inform. Eng.*, vol. 6. Los Angeles, CA, pp. 469 – 473.

[36] G. Song and R. Zhao, "Three novel models of threshold estimator for wavelet coefficients," in *Lecture Notes in Computer Science: Wavelet Analysis and Its Applications*, vol. 103, Y. Y. Tang *et al.*, Eds., New York: Springer-Verlag, 1994, pp. 125 – 150.

[37] Physionet, "PhysioBank ATM", available online, http://www.physionet.org/ cgi-bin/ATM.

[38] Physionet, "The MIT-BIH arrhythmia test database", available online, http:// www.physionet.org/physiobank/database/mitdb.

[39] Physionet, "The MIT-BIH noise stress test database", available online, http://www.physionet.org/physiobank/database/nstdb.

[40] V. K. Pandey and P. C. Pandey, "Tracking-based baseline restoration circuit for acquisition of bio signals," *Electronics Letters*, vol. 43, no. 6, pp. 13 – 14, 2007.

[41] D. L. Donoho, "De-noising by soft-thresholding," *IEEE Trans. Inform. Theory*, vol. 41, pp. 613 – 627, 1995.

[42] T. Sebastian, P. C. Pandey, and V. K. Pandey "Wavelet based denoising for suppression of respiratory and motion artifacts in impedance cardiography," in *Proc. Int. Conf. Computing in Cardiology*, Sept. 18 – 21, 2011, Hangzhou, China [accepted].

[43] P. Mithun, P. C. Pandey, T. Sebastian, P. Mishra, and V. K. Pandey, "A wavelet based technique for suppression of EMG noise and motion artifact in ambulatory ECG," in *Proc. 33rd Ann. Int. Conf. IEEE Eng. Med. Biol. Soc*., Aug. 30 – Sept. 3, 2011, Boston, MA [accepted].

Acknowledgement

I am grateful to Prof. P. C. Pandey for giving me an opportunity to work under his esteemed guidance for my M. Tech Project. I would like to express my deep gratitude for his valuable suggestions and constant encouragement throughout the project.

I thank Dr. Vinod Pandey, P. Mithun, and S. M. M. Naidu for their support and critical inputs throughout the project. I would also like to express my sincere thanks to all my labmates for their unstinted help and support during the project work. I am also thankful to my batchmates, Shailesh and Thirupathi, for making the life in IIT unforgettable.

I am highly indebted to my parents, Tania, Thomas, and Betty for all the moral support during my studies.

Toney Sebastian

Author's Resume

Toney Sebastian: He received the B. Tech. degree in electronics and communication engineering from Cochin University of Science and Technology, Cochin (Kerala) in 2007. He worked as a Lecturer at Acharya Institute of Science and Technology, Bangalore during June to December 2008. Presently, he is pursuing the M.Tech. degree in biomedical engineering at the Indian Institute of Technology Bombay. His research interests include embedded system design, digital signal processing, and wavelets.

Thesis related publications

T. Sebastian, P. C. Pandey, and V. K. Pandey "Wavelet based denoising for suppression of respiratory and motion artifacts in impedance cardiography," in *Proc. Int. Conf. Computing in Cardiology*, Sept. 18 – 21, 2011, Hangzhou, China [accepted].

P. Mithun, P. C. Pandey, T. Sebastian, P. Mishra, and V. K. Pandey, "A wavelet based technique for suppression of EMG noise and motion artifact in ambulatory ECG," in *Proc. 33rd Ann. Int. Conf. IEEE Eng. Med. Biol. Soc.*, Aug. 30 – Sept. 3, 2011, Boston, MA [accepted].